RADC-TR-78-252
Final Technical Report
November 1978

ANALYSIS OF TROPOSPHERIC EFFECTS AT LOW ELEVATION ANGLES

Environmental Research & Technology, Inc.

Robert K. Crane

Approved for public release; distribution unlimited.

ROME AIR DEVELOPMENT CENTER
Air Force Systems Command
Griffiss Air Force Base, New York 13441

AUG 27 1979

A

79 08 24 007

This report has been reviewed by the RADC Information Office (OI) and is releasable to the National Technical Information Service (NTIS). At NTIS it will be releasable to the general public, including foreign nations.

RADC-TR-78-252 has been reviewed and is approved for publication.

APPROVED: *Uve H. W. Lammers*

UVE H. W. LAMMERS
Project Engineer

APPROVED: *Allan C. Schell*

ALLAN C. SCHELL, Chief
Electromagnetic Sciences Division

FOR THE COMMANDER: *John P. Huss*

JOHN P. HUSS
Acting Chief, Plans Office

If your address has changed or if you wish to be removed from the RADC mailing list, or if the addressee is no longer employed by your organization, please notify RADC (EEP) Hanscom AFB MA 01731. This will assist us in maintaining a current mailing list.

Do not return this copy. Retain or destroy.

REPORT DOCUMENTATION PAGE		READ INSTRUCTIONS BEFORE COMPLETING FORM
1. REPORT NUMBER RADC-TR-78-252	2. GOVT ACCESSION NO.	3. RECIPIENT'S CATALOG NUMBER
4. TITLE (and Subtitle) ANALYSIS OF TROPOSPHERIC EFFECTS AT LOW ELEVATION ANGLES .		5. TYPE OF REPORT & PERIOD COVERED Final Technical Report, 1 Jan 77 - 31 May 78
		6. PERFORMING ORG. REPORT NUMBER N/A
7. AUTHOR(s) Robert K. Crane		8. CONTRACT OR GRANT NUMBER(s) F19628-77-C-0074
9. PERFORMING ORGANIZATION NAME AND ADDRESS Environmental Research & Technology, Inc. 696 Virginia Road Concord MA 01742		10. PROGRAM ELEMENT, PROJECT, TASK AREA & WORK UNIT NUMBERS 62702F 46001621
11. CONTROLLING OFFICE NAME AND ADDRESS Deputy for Electronic Technology (RADC/EEP) Hanscom AFB MA 01731		12. REPORT DATE November 1978
		13. NUMBER OF PAGES 67
14. MONITORING AGENCY NAME & ADDRESS(if different from Controlling Office) Same		15. SECURITY CLASS. (of this report) UNCLASSIFIED
		15a. DECLASSIFICATION/DOWNGRADING SCHEDULE N/A

16. DISTRIBUTION STATEMENT (of this Report)

Approved for public release; distribution unlimited.

17. DISTRIBUTION STATEMENT (of the abstract entered in Block 20, if different from Report)

Same

18. SUPPLEMENTARY NOTES

RADC Project Engineer: Uve H. W. Lammers (EEP)

19. KEY WORDS (Continue on reverse side if necessary and identify by block number)

refraction errors
refraction effects
tropospheric propagation
low elevation angle propagation
Millstone radar

20. ABSTRACT (Continue on reverse side if necessary and identify by block number)

Precision low elevation angle radar observations of orbiting spheres were used to evaluate the utility of surface based refraction techniques. Elevation angle error measurements were obtained from differences between the precision radar measurements and the true or absolute position of the orbiting sphere obtained from a multiple pass orbit determination using data from the same radar system. The results of the refraction effects study show that the average observed elevation angle error caused by refraction is identical with the average calculated elevation angle error obtained from ray tracings using radiosonde data to within

DD FORM 1 JAN 73 1473

391 776

the measurement accuracy of the radar system. The results also reveal a relatively large uncorrectable component of the elevation angle error caused by small scale refractive index gradients. This uncorrectable component is of the order of 30 millidegrees (mdeg) at a true elevation angle of 1 degree and 4 mdeg at 10 degrees.

EVALUATION

1. This document is the Final Report on the contract which over the period from January 1977 to May 1978 investigated tropospheric effects on low elevation angle ray paths. The report describes the data collection, verification and analysis leading to a set of final conclusions which are extremely valuable to radar system designers and users. Today's precision radar systems require accurate tropospheric refraction corrections to account for the time delay and ray path bending due to the lower troposphere. The question arises: Is the state of the art in tropospheric refraction predictions such that further advances in radar equipment accuracy will yield little or no system accuracy improvement due to tropospheric prediction errors? The results of this contract provide the answer. For elevation angles below twenty degrees, the fluctuations due to large and small scale atmospheric processes result in residual errors which cannot be reduced by either surface based or radiosonde observations. These residual errors are larger than predicted by simulation and result in less improvement in the prediction of tropospheric refraction errors using surface data than expected.

2. The inescapable conclusion of this effort is the existence of a lower bound in the prediction accuracy of tropospheric refractive effects which cannot be crossed without a vast increase in the knowledge of the instantaneous state of the lower atmosphere. The use of surface refractivity as a predictor results in errors very close to the lower bound and this accounts for the relatively small improvement derived from the use of more complex refraction prediction schemes.

3. The results of this contract will be of interest to radar system users and designers who are contemplating systems with angular accuracies approaching the lower bound described above.

Larry E Telford

LARRY E. TELFORD
Alternate Contract Monitor
Propagation Branch
Electromagnetic Sciences Division

iii

TABLE OF CONTENTS

LIST OF ILLUSTRATIONS

LIST OF ILLUSTRATIONS (cont)

LIST OF TABLES

1. INTRODUCTION

1.1 Objective

The objective of this contract is an evaluation of the adequacy of surface based methods for the estimation of refraction effects at low elevation angles. A number of simulations of refraction effects have been performed using ray tracing techniques which have resulted in procedures for the correction of refraction induced errors (Bean et al, 1960; Crane, 1976a). Adequate experimental verification of the correction procedures, however, was not available. As one of the end products of a large scale radar propagation experiment, Lincoln Laboratory, MIT amassed a number of precision radar tracks of orbiting spheres sufficient for the testing of refraction correction algorithms (Evans, 1973a; Crane, 1976b).* These data were analyzed under this contract to experimentally determine refraction induced elevation angle errors at low elevation angles and to evaluate the utility of a statistically derived correction procedure based on the use of surface refractivity observation.

1.2 Summary of Results

Precision radar tracks of orbiting calibration spheres were analyzed to provide statistical estimates of refraction induced elevation angle errors and the residual errors remaining after correction based on surface refractivity observations. The elevation errors were estimated from differences between radar observed sphere positions and the "true" or absolute positions of the sphere obtained by calculation from the orbital elements for each sphere. Precise reference orbits were established for each sphere using multiple pass radar observations and a specially developed non-real-time-precision orbit determination program, ORBFIT (see section IV, Evans, 1973b; TRW, 1966).

---

* Radar tracking data and precise orbit data were provided courtesy of Dr. J.V. Evans of Lincoln Laboratory.

The results of this refraction analysis study are presented in Tables 1 and 2. The true elevation angle is the straight line (unrefracted) direction to the sphere. The observed elevation error is the refraction induced pointing angle error; the radar observed the sphere at an apparent elevation angle too high by the observed elevation angle error. The expected elevation angle error is the result of computer simulation by ray tracing. The average observed and expected values differ by at most 3.2 percent and are generally within 2 percent for elevation angles below 10 degrees. The results show excellent agreement between observation and simulation; the differences are within the measurement error of the Millstone L-band radar system. Based on these results, it is evident that surface refraction correction procedures can reduce the average elevation angle error.

Table 2 presents the root mean square (rms) deviations of the elevation errors about the mean value or about the estimated elevation angle correction calculated using the simultaneously observed value of surface refractivity. Earlier work by Crane (1976b) showed that short term, random fluctuations in elevation angle were of the same order of magnitude as the expected day-to-day variations (expected residual after correction). In that work, only deviations about the detrended elevation angle were considered; bias or average refraction effects were ignored and only the random fluctuations were analyzed. In this study, the rapidly fluctuating components of the elevation angle error were removed by averaging and only the slowly varying or bias values are considered. The observed deviations are from one 20-second observation interval to the next and from one satellite pass to the next; they represent the random variation of the bias component of the refraction error. The observed fluctuations about the mean range from equal to nearly 1.4 times the expected (simulated) value, as shown in Table 3. The observed residual after correction ranged from 2.5 to 7.4 times the expected value; the reduction in rms deviation was by less than a factor of 1.7 while the expected reduction was by a factor of 5.9 or better at elevation angles above 1°.

The surface correction procedure reduced the rms deviations by as much as was possible for the given set of surface refractivity values. The correlation between the residual elevation angle after correction

TABLE 1

AVERAGE VALUES

True Elevation Angle (deg)	Observed Elevation Error (mdeg)	Expected Elevation Error (mdeg)	Residual Elevation Angle Error		Number of Samples	Surface Refractivity N_s (N - units)	Correlation Coefficient ε vs N_s
			ε (mdeg)	(percent of expected)			
0.5	531	523	-3.0±6.4	1.5	23	343	0.01±0.2
1.5	376	374	-1.7±3.3	0.4	53	335	0.02±0.1
2.5	285	291	6.3±5.2	2.1	101	330	0.07±0.1
3.5	233	241	7.9±1.6	3.2	128	332	0.09±0.09
4.5	194	197	3.4±1.1	1.7	163	331	0.002±0.08
5.5	167	170	2.5±0.9	1.5	158	334	0.007±0.08
6.5	147	150	3.1±0.8	2.1	200	334	0.16±0.07
7.5	129	132	2.5±0.7	2.1	191	333	0.004±0.07
8.5	114	116	2.0±0.6	1.7	185	332	0.000±0.07
9.5	105	105	0.2±0.6	0.2	170	335	-0.03±0.08
10.5	94	94	0.3±0.6	0.3	165	331	0.005±0.08

TABLE 2

ROOT MEAN SQUARE DEVIATIONS

True Elevation Angle (deg)	Observed Elevation Angle Deviation About Mean (mdeg)	Expected Elevation Angle Deviation About Mean (mdeg)	Observed Residual After Correction (mdeg)	Expected Residual After Correction (mdeg)
0.5	51.5	52	30.1	12.2
1.5	38.8	31	23.9	5.3
2.5	31.0	22	22.1	3.0
3.5	23.6	17	17.1	2.6
4.5	17.6	14	11.7	2.1
5.5	13.9	11.6	9.3	1.7
6.5	12.1	10.0	8.3	1.5
7.5	9.5	8.9	5.9	1.3
8.5	8.4	7.8	5.2	1.1
9.5	6.6	7.1	4.3	1.0
10.5	6.4	6.4	3.2	0.9

4

TABLE 3

REDUCTION OF VARIANCE
(RATIOS OF RMS DEVIATION VALUES)

True Elevation Angle Deg	$\dfrac{\text{Observed}}{\text{Expected}}$ Variation About Mean Value	$\dfrac{\text{Observed}}{\text{Expected}}$ Variation About Correction	$\dfrac{\text{Mean}}{\text{Residual}}$ Observed	$\dfrac{\text{Mean}}{\text{Residual}}$ Expected	Correlation Coefficient Observed Error vs N_s
0.5	1.0	2.5	1.7	4.3	0.65
1.5	1.3	4.5	1.6	5.9	0.61
2.5	1.4	7.4	1.4	7.3	0.49
3.5	1.4	6.6	1.4	6.5	0.49
4.5	1.3	5.6	1.5	6.7	0.56
5.5	1.2	5.5	1.5	6.8	0.56
6.5	1.2	5.5	1.5	6.7	0.56
7.5	1.1	4.5	1.6	6.9	0.61
8.5	1.1	4.7	1.6	7.1	0.61
9.5	0.9	4.3	1.5	7.1	0.56
10.5	1.0	3.6	2.0	7.1	0.75

5

and the surface refractivity value used for correction was not signifi-
cantly different from zero (see Table 1; the confidence intervals are
for 67 percent included or 1 standard deviation, 1 σ). This result,
obtained from a sample of over 1500 bias elevation angle error observa-
tions, shows that although the correction technique did well on average,
considerable error may still exist for a particular pointing angle obser-
vation. The surface correction scheme did not work as well as expected
based on the simulation analysis. Since the earlier analysis of Haystack
observations (Crane, 1976b) indicated that the random fluctuations about
a detrended elevation angle value were of the order of the expected
residual values and that increased fluctuations should occur when larger
observing intervals in either time or elevation angle were used, the
larger random fluctuations for the larger elevation angle spans of the
Millstone observations were expected. These larger fluctuations are
random in nature and not accessible to correction using surface values.
The observed rms deviations after correction represent the limitations
of surface correction procedures.

Subsequent sections of this report provide a brief background for
the measurement program, a description of the observations and ray trac-
ing simulations and an analysis of the results. Section 2 places the
measurement program in context. Section 3 describes the Millstone Hill
L-band measurement program. Section 4 describes the simulation proce-
dure and the ray tracing procedure used for the calculation of refraction
effects. Section 5 presents the comparison between observations and
expectations and Section 6 summarizes the conclusions.

6

2. BACKGROUND

2.1 Prior Studies

Radar systems operating within the troposphere have long experienced measurement errors caused by spatial and temporal variations in the index of refraction of the air. Although the phenomenon was well known, refraction induced errors were not of consequence for most radar systems operating prior to 1960 with the exception of height finders. A number of simulation studies were made in the late 1950's to evaluate the seriousness of refraction induced errors and to provide possible procedures for refraction correction (Bean and Thayer, 1954, Bauer et al, 1958; Bean et al, 1960). From these studies it became evident that the calculated values of ray bending and of elevation angle error were highly correlated with the surface value of the index of refraction or surface refractivity. Bean et al [1960] provided tables for the statistical correction of elevation angle errors using surface refractivity measurements. The correction values were estimated using a linear relationship between elevation angle error (or bending) and surface refractivity. The coefficients for use in these relationships were derived from linear regression analysis of simulated errors and surface refractivity values. The ray tracings used for the simulations were calculated based on a 77 profile sample representing six different refractivity profile types for 13 climate regions.

The use of the statistical prediction technique had not been experimentally verified. Bean and Thayer [1963] reported on the use of the statistical model and provided samples of comparisons between simulations and observations. Their most convincing comparison with experiment was with the measurements performed by Anway [1963] using a 2-cm wavelength radio sextant. The results reported by Anway differed from the mean values of elevation angle error estimated using the 77 profile sample by less than the standard deviation of the observations. Anway also reported on the correlation between observed elevation angle error and surface refractivity. He calculated a correlation coefficient of 0.87 for observations at an apparent elevation angle of 8°, sufficient to reduce the rms deviations by a factor of 2.8 using the surface correction

7

procedure. The measured correlation coefficient was not as high as the value calculated by Bean et al, a value in excess of 0.99 at an apparent elevation angle of 8°. However, the results were very encouraging and refraction correction based on surface refractivity values have been used in radar system operation at low elevation angles. Recently, in an investigation of the effects of large scale horizontal variations in refractive index profiles, Gallop and Telford (1975) simulated the effects of horizontal inhomogeneity and reported that correction based on only surface refractivity measurements would not be as successful as expected for a horizontally homogeneous atmosphere. They suggested that the effects of horizontal variation would be small at a 5° elevation angle and negligible at 10°, not sufficient to explain the Anway results.

2.2 Millstone Hill Radar Propagation Study

In 1969, Lincoln Laboratory began a joint study with the Bell Telephone Laboratory to investigate the limitations imposed by naturally occuring propagation effects on defensive radar systems operating at UHF (Evans, 1973a). The initial objective of the joint study was to evaluate the effects of the auroral region of the ionosphere on radar system performance. Refraction effects associated with the auroral region were expected to be important at UHF but not at L-band. Accordingly, a two frequency measurement program was devised to use the Millstone Hill L-band radar for observations of UHF beacon satellites to provide reference position information and a newly developed UHF tracker on the same antenna for observations of the angle-of-arrival of the signals from the beacons. As the program developed and more stringent accuracy requirements were placed on locating the absolute position of the beacon, the use of the L-band radar for reference position determination based on single radar observations was abandoned.

An extensive development program was undertaken to provide a measurement and analysis system capable of accurately determining the orbits of the beacon satellites. With precise orbital information, the absolute location of the satellite could be determined and tracking perturbations induced by the ionosphere could be determined by comparing the observed position with the calculated position. To accomplish the task of obtaining an accurate reference orbit for a satellite, the satellite

8

was observed over many successive passes over the radar station and the orbital equations were solved using a non-real-time-precision orbit determination program to establish the best fit reference orbit consistent with orbital mechanics and a large number of radar observations. An extensive radar calibration program was undertaken to provide models for all known sources of errors in the L-band radar observations. The errors had to be modeled and corrected prior to use in the orbit fitting program to provide the best possible data for the determination of the reference orbit (Evans, 1973b).

As a part of the L-band radar calibration and error modeling program, a surface refractivity correction scheme was developed that was tailored to the Millstone radar climate (northeastern Massachusetts). The statistical procedure developed by Bean et al (1960) was based on a limited number of profiles representing extreme conditions in a number of different climate regions. A new regression analysis was undertaken (Evans, 1969; Crane, 1976a) using radiosonde data from two months (February and August) of each of three years for Albany, New York, a location with a climate similar to Millstone Hill. The new statistical parameters were expected to be better than the earlier model because the parameters were from a statistical analysis using a sample population which represented the population to be expected at observation time. The surface refractivity correction procedure was used without experimental verification throughout the joint study measurement program, 1970-1973. The regression coefficients for use at low elevation angles were modified in 1972 to reduce differences between the statistically predicted bending values and ray-tracing calculations for four soundings obtained with a nearby radiosonde.

The joint propagation study was concluded in March 1973 and a follow-on tropospheric refraction effects study was begun by Lincoln Laboratory for the U.S. Army Advanced Ballistic Missile Defense Agency (ABMDA). The tropospheric effects measurement program was conducted in two phases, the first a series of L-band radar observations conducted in sixteen tracking sessions between 1 October 1973 and 30 September 1974 for the purposes of measuring the bias refraction errors and evaluating the surface refractivity correction procedure and the second a series of measurements of the random fluctuations in amplitude and angle-of-arrival

9

caused by refractive index inhomogeneities in the lower troposphere.
The random fluctuation or scintillation observations were made during
1975 and have been reported by Crane (1976b). The L-band observations
were processed through the determination of the reference orbits for
each of the spheres tracked during the last four tracking sessions but
the data were not analyzed further due to changing priorities both in
the Army and at Lincoln Laboratory.

This report presents the results of the analysis of the bias refrac-
tion data obtained during the last two tracking sessions, during Septem-
ber 1974. The completion of the analysis has been supported by the U.S.
Air Force, Rome Air Development Center to provide experimental verifica-
tion of the use of surface refraction correction techniques for the cor-
rection of elevation angle errors at low elevation angles.

3.   PRECISION REFRACTION EFFECTS MEASUREMENT

3.1   L-band Radar Systems

The Millstone Hill L-band radar system has been described
by Ghiloni [1973]. The radar system is a high powered, monopulse
tracker. For satellite tracking operations, the radar system was
nominally operated at a 3.3. MW peak power and 100 KW average power.
A 2-millisecond pulse was used at a pulse repetition frequency of 15 pps.
The radar utilizes a Cassigrain antenna system with a 25.6m (84-ft.)
diameter aperture. At the operating frequency of 1295 MHz, the antenna
has a gain of about 47 dB with a 0.7 degree half power beamwidth (one-
way). The transmitted polarization was right-hand circular.

The receiver system employs a 12-horn monopulse tracking feed
to develop the sum and difference signals required for detection and
tracking. The left-hand circular polarization sum channel signals were
processed through low noise RF amplifiers, several stages of IF processing
and were both coherently and incoherently detected. The in-phase and
quadrature signal amplitude values and the normalizing amplifier AGC
output were digitally recorded for use in computer-aided real-time sat-
ellite tracking (using the CAST program, see Evans 1973b) and for post
mission analysis. The elevation and azimuth difference signals in-phase
with the sum signal were normalized using the AGC output to derive
pointing angle error values which were digitized and input to the on-site
SDS 9300 computer for real-time tracking and storage for post test analysis.
The radar signals were processed in real-time and used to develop
tracking commands to steer the antenna, the range gate, and the Doppler
frequency offset to control one of the IF frequencies. The antenna posi-
tion encoder values were also processed by the computer and used to
generate the new pointing commands; the tracking loops were closed through
the computer.

Auxilliary data for pointing error correction were also sam-
pled and processed through the computer. The surface refractivity was
measured by a microwave refractometer mounted on the outside wall of the
radar equipment shelter attached to the antenna and it was positioned at
roughly the height of the phase center of the antenna when operating at

11

low elevation angles. The refractivity values were averaged for 1000 seconds prior to recording to remove small scale turbulent fluctuations in the refractivity values. The tilt of the antenna tower was also measured and recorded for use in removing the effects of mechanical deformation of the antenna supporting structure. The deformation of the tower caused by solar heating often exceeded 20 mdeg and required compensation to provide angle-of-arrival measurements of sufficient accuracy to determine refraction effects. Tower tilt was measured by two orthogonally oriented electronic level sensors, the principal tilt measurement was in the elevation plane of the antenna.

The Computer Aided Satellite Tracking program (CAST) was an integral part of the L-band radar tracking system used for the low elevation angle refraction measurements. This program, resident in the SDS 9300 computer, closed the tracking loops used to steer the antenna, range gate, and Doppler offset. Single L-band radar returns were not sufficiently noise-free for precision satellite tracking. Accordingly, a tracking procedure was devised to use the radar observations to correct the calculated satellite ephemeris values; the radar data were smoothed and used to differentially adjust the predicted satellite position. In this way, a significant amount of smoothing could be used to reduce radar measurement uncertainty. The CAST program also removed known, modeled measurement errors caused by refraction, tower tilt, encoder offsets, feed droop (change in the electrical axis of the antenna relative to the mechanical axis caused by mechanical deformation of the antenna as the antenna elevation angle is changed), beam collimation and non-perpendicularity of the elevation and azimuth axes. The smoothed differences between the ephemeris values and the best estimate, corrected radar position observations were used to correct the ephemeris values to provide the tracking commands.

The raw data were corrected to provide best estimate azimuth and elevation angle values. The corrections used were:

$$AZ' = AZ_{enc} + ABIAS_r + ASLOPE_r \times AZ_{enc}$$

$$AZ'' = AZ' + \sin(TILT) \times \sin(TILTAZ - AZ') \times \tan(EL_{enc})$$

$$EL' = EL_{enc} - \sin(TILT) \times \cos(TILTAZ - AZ')$$

$$EL'' = EL' + [1 - \cos(TILT)] \times \tan(EL_{enc})$$

12

$$EL''' = EL'' - EBIAS + \Delta EL - ELSLOPE \times EL''$$

$$EL'''' = EL''' - (A + B \times N_s)$$

$$\Delta AZ = [\Delta TRAV + COLL - SKEW \times \sin(EL''')]/\cos(EL''')$$

$$AZ''' = AZ'' - ABIAS + \Delta AZ$$

where AZ_{enc} and EL_{enc} are the azimuth and elevation angle encoder values, $ABIAS_r$ and $ASLOPE_r$ provide the corrections for known deficiencies in the azimuth encoder system, TILT and TILTAZ are the principal and orthogonal tilt meter readings, EBIAS and ELSLOPE correct for deficiencies in the elevation encoder system and feed droop, N_s is surface refractivity, ΔEL and $\Delta TRAV$ are the elevation and traverse (azimuth) error signals derived from the monopulse difference channels, COLL and SKEW correct for collimation and non-perpendicularity between azimuth and elevation axes and ABIAS corrects for misalignment of the azimuth reference direction. These corrections were made in real-time by the CAST program and the required auxiliary data and model parameters were recorded for further refined post mission analysis. The raw radar data together with the best estimate corrected, edited, and smoothed observations used for tracking were recorded for post mission analysis. The smoothing parameters could be changed easily. For the observations of interest to this report smoothing was accomplished by least square fitting of data from successive non-overlapping 20-second periods to third degree polynomials and reporting the value from the fitted curve at the midpoint of the inverval. L-band tracking data obtained during the joint study and the first half of the 1973-1974 low elevation angle tracking study were obtained using an eight-second smoothing interval.

3.2 Orbit Estimation

The smoothed data were processed by the multipass orbit determination program, ORBFIT (Evans, 1973b), to determine best estimate reference orbits for use in estimating refraction effects. Data for a single satellite were acquired from each successive pass of the satellite visible to Millstone Hill radar during a five to seven day tracking period. The data were from different directions relative to the radar station and represent orbital motions in different directions relative

13

to the radar site. The smoothed data included the corrected, observed position estimate for each smoothing interval and the rms deviations of the raw data about the polynomial curve used in the smoothing operation. The rms data were used to establish the relative quality of the smoothed observations; the reciprocal of the rms deviation value was used to weight the observation in the least squared determination of the best estimate state vector for the satellite orbit. The ORBFIT program also provided best estimate fixed bias estimates (EBIAS, ABIAS) as well as the orbital elements.

ORBFIT integrates the Keplarian equations of motion for a satellite in the gravitational force field of the Earth. Although capable of being considered, ORBFIT, as operated for the analysis of low angle tracking data, ignored the effects of atmospheric drag, solar radiation pressure, and perturbation of the orbit by the Sun and Moon. The Earth and gravitational force model employed for orbit determination was the DOD WGS-66 model (DOD, 1966). ORBFIT used differential correction to estimate the state vector.

The use of ORBFIT to provide precise reference orbits was verified by comparison with the Naval Weapons Laboratory (NWL) precise orbital ephemeris for one of the Navy Navagation System Satellites (NNSS). The NNSS were used as the beacon sources for the UHF measurements obtained during the joint study (Evans, 1973a). The NWL data were derived from multi-station Doppler tracking data and were processed in an orbit determination program that included the effects of drag, solar radiation pressure, Sun-Moon perturbations, and higher order geopotential terms than used in ORBFIT. L-band radar observations for nine passes of the NNSS SPACETRACK Object No. 2965 from the 8-11 August 1972 tracking session were processed through ORBFIT for comparison with the NWL data. NWL ephemeris data at one minute intervals for the sections of the orbit visible to Millstone Hill produced the following rms residuals when compared with the ORBFIT reference orbit: range 92m, azimuth 13 mdeg, elevation 1 mdeg. When ORBFIT was allowed to adjust the orbit to the NWL data, the rms residuals were reduced to 20m, 1.6 mdeg, and 0.3 mdeg respectively. These latter numbers are a measure of the ORBFIT program analysis errors; the former are a measure of the state of radar calibration in 1972.

14

3.3 Calibration

An extensive radar calibration program was undertaken as a part of the Lincoln Laboratory-Bell Telephone Laboratory joint study program and was continued through the period of the low elevation angle tropospheric refraction effects study. The calibration program resulted in a continuous upgrading of the error models for the facilities and in the observation procedures used during the tracking sessions.

Angle-error channel calibration data were obtained on each satellite pass that rose higher than about 10° above the horizon. After the first few smoothed data samples are available to the CAST program, an optional ephemeris update can be performed to provide best estimate position data consistent with the initially entered state vector for the orbit and the accumulated observations for the pass. At relatively high elevation angles during a satellite pass, error signal calibration is affected by offsetting the antenna in elevation then in azimuth by a predetermined angle from the computed best estimate satellite location. Offsets are provided in both positive and negative directions and the calibration values for the error channels (EL and TRAV) are determined from the change in error signal versus the change in pointing angle.

Direct azimuth calibration measurements were made periodically using optical sightings of fixed reference targets and a boresight telescope. The azimuth encoder system could not be directly mounted on a rotating shaft due to the azimuth rotary joint structure. An elaborate, octagon within an octagon cam follower system was constructed to provide a shaft on the inner octagon that rotated once per revolution of the main antenna. The accuracy of the reported azimuth position depended on the precision of the location of the rails used to provide the outer octagon surface. This system required separate modeling of the errors introduced by the eight rails in the system requiring the determination and monitoring of eight separate $ABIAS_r$ and $ASLOPE_r$ calibration constants. Analysis of a number of optical target sightings revealed that the cam follower, encoder system had an rms error of 4.2 mdeg about the calibration model.

The tilt meter system also was evaluated by direct calibration means. Each meter was tilted by a known amount and the electronic system was adjusted to provide a nominal angle-to-volt calibration constant. An

15

indirect calibration procedure was also devised to measure the response of the tilt meters without mechanically disturbing the tilt meters. The antenna was rotated while pointed in a vertical direction. With the antenna in this orientation, the tower should not be deformed by antenna motion and the output of the tilt meters should be sinusoidal functions of azimuth. The departure of the tilt meter outputs from the expected sinusoids was taken as a measure of the error of the tilt meter system. In particular, d.c. offsets could be readily detected with this procedure as well as changes in the response of one tiltmeter relative to the other. As operated, it is expected that tower tilt can be reliably measured to within 3 mdeg.

The overall calibration of antenna pointing biases were made using radio star observations. Radio star positions of sources suitable for L-band system calibration are known to within about 3 mdeg. The L-band monopulse tracking receiver system was modified to enable wide bandwidth (1 MHz) sum and difference channel radiometer observations of the radio stars. The computer commanded the antenna to track the radio sources and to provide offset calibration scans. Monopulse tracks of the radio sources Cassiopeia A, Cygnus A, and Taurus were periodically obtained during nighttime hours to eliminate interference from the sun. Calibration measurements made with sources in different positions in the sky were combined to solve for the coefficients of the error models: for elevation and azimuth biases, collimation, skew, and feed droop. Typical rms uncertainties in the determination of the radio star positions after removal of the modeled errors are the order of 5 mdeg in azimuth and 3 mdeg in elevation. Radio star observations were made periodically during the measurement program to monitor the error model coefficients.

Finally, the ORBFIT program provided bias error estimates as well as statistical information on the residual differences between the corrected and smoothed radar data and the estimated orbit. Some of the errors such as feed droop could be monitored by repeated runs of the program with different values for the parameter to be investigated. The best value for the parameter would consistently yield the smallest residual rms deviations for several different satellites.

Intercomparisons between the ORBFIT orbital estimates and the smoothed radar observations made toward the end of the joint study when

the calibration procedures were most advanced and when the best models for the error sources were used yielded rms elevation angle residuals of the order of 6 mdeg and azimuth residuals of about the same magnitude. In particular, for all the satellites tracked during the 27-30 March 1973 tracking session, the elevation residuals obtained using an 8-second smoothing interval were 6.1±0.3 mdeg and the azimuth residuals were 6.4±0.5 mdeg; for the previous tracking session, intercomparison between the ORBFIT orbit and the NWL orbit for one of the NNSS yielded rms differences of 1.6 mdeg in elevation and 3 mdeg in azimuth.

During the 1973-1974 time period, additional modifications were made to improve system calibration. The originally provided refraction correction coefficients were reintroduced into the correction procedure to provide a broader based statistical correction using the observed surface index values. Tracking with fixed offsets was introduced to provide higher signal to noise levels for the calibrated error signals. The operation of the normalizing amplifier was improved to reduce uncertainties in the cross section value and in the error signal value. Coherently detected in-phase and quadrature amplitude values were also recorded for the sum channel signal to provide post analysis verification of the normalization amplifier AGC output and to provide an independent, well-calibrated, cross section measurement. The data used by ORBFIT was constrained to lie between 5 and 40° elevation angle to reduce uncertainties caused by rapid antenna motion at higher elevation angles and by refraction effects at lower angles. This last step removed the possibility of having the best fit orbit affect the determination of refraction errors by adjusting the orbit to compensate for any errors that remained after surface index correction. The final results for tracks of 0.1, 0.2, and 1.0 m^2 cross section spheres were rms elevation residuals relative to the reference orbits of 6.0±0.2 mdeg for the 1 m^2 sphere, 6.8±0.2 mdeg for 0.2 m^2 spheres and 7.4±0.2 mdeg for 0.1 m^2 cross section spheres.

3.4 Sample Observations

Orbiting spheres were used to provide the majority of satellite tracks during the last four tracking sessions of the 1973-1974 measurement period. Sphere data were selected for analysis because they were not subject to the angular errors caused by glinting (interference

between scattered signals from a complex target within the same range, beam width resolution cell). Figures 1 and 2 provide samples of the smoothed output data provided for single satellite passes by the CAST program. Figure 1 is for a more complex target with a large cross section but with obvious angle-of-arrival fluctuations at all elevation angles. By way of contrast, Figure 2 displays the CAST output data for a 1 m^2 cross section sphere (the Lincoln Calibration Sphere, LCS-4, SPACETRACK Object No. 5398). The cross-section and angle-of-arrival fluctuations are not evident except at low elevation angles. Since the sphere does not adversely affect the cross-section or angle-of-arrival measurements, it provides an ideal target for refraction effects analysis. Unfortunately, the cross-sections of the spheres available as targets are relatively small and considerable smoothing (20 seconds) is required to reduce the effects of receiver noise.

Two types of data were generated by the CAST program, smoothed data used by ORBFIT for orbit determination and raw data for use in post processing. Figure 3 presents a sample output for a one minute segment of a track of a 1 m^2 cross-section sphere at low elevation angles. The figure displays the cross-section values measured in decibels relative to a 1 square meter cross-section value (dBsm) and the elevation and traverse [azimuth cos(elevation)] angle differences between the reference orbit and the corrected radar return versus elapsed time and true (corrected) elevation angle. Data for each radar return (each pulse) are displayed. The rapid angle fluctuations are caused by receiver noise. The expected rms angle fluctuation is given by

$$\Delta\Theta = \frac{\Theta_o}{n\ (S/N)} \tag{1}$$

where Θ_o is halfpower beamwidth (one way), n is the number of independent samples averaged to determine the pointing angle, Θ, (S/N) is the signal-to-noise ratio and $\Delta\Theta$ is the rms angle uncertainty. For the data displayed on the figure, the rms angle-of-arrival fluctuations are between 20 and 30 mdeg rms. From equation (1), the signal-to-noise ratio for a beamdwidth of 0.7 degrees and a 30 mdeg rms noise induced fluctuation is 27 dB. The sum channel S/N at the same time was the order of 35 dB. With the tracking offset used to increase the signal level in the error channels, a 27 dB S/N for the error channel is reasonable. Using a
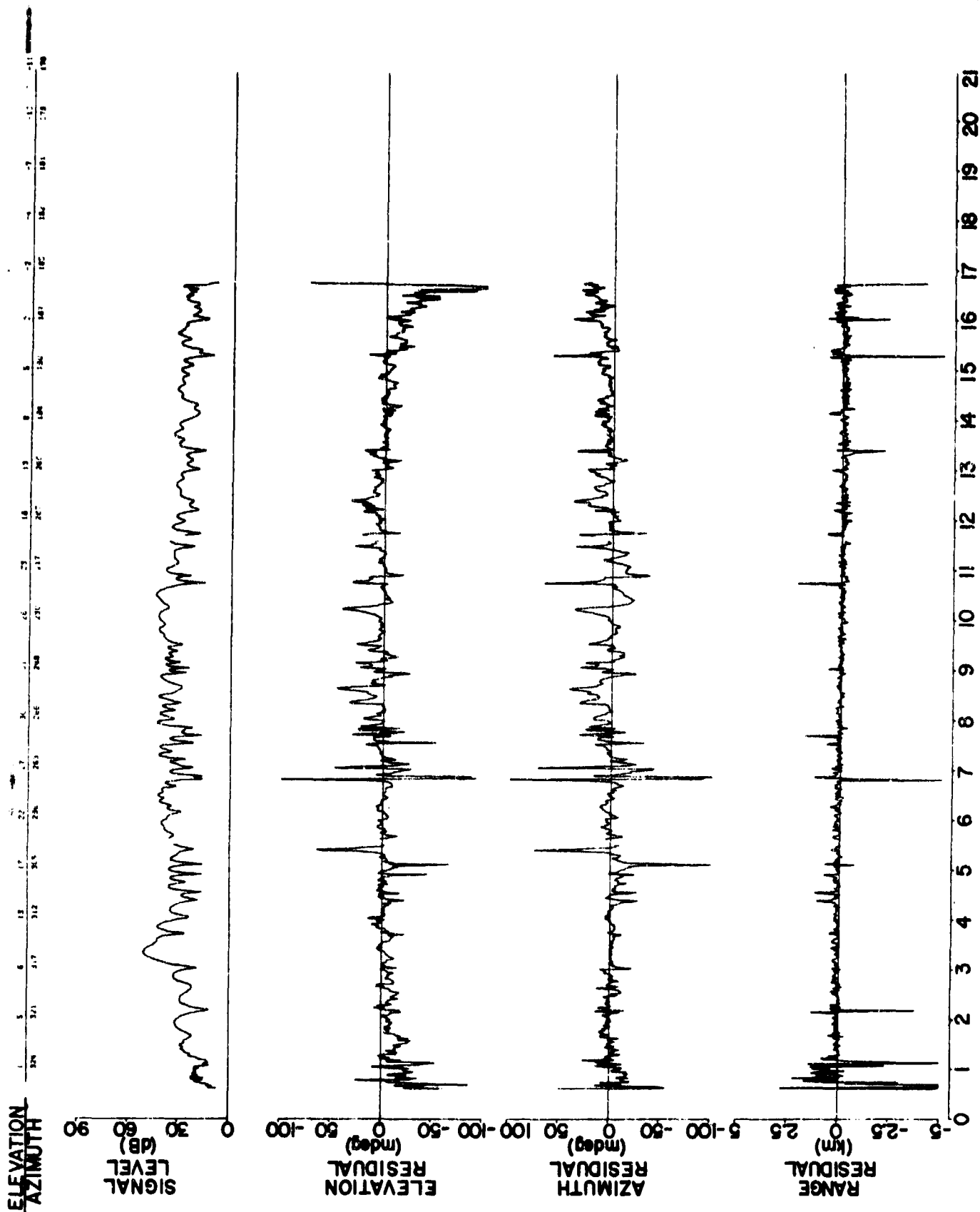
18

Figure 1 CAST summary output data for track of cylindrical object SPACETRACK object No. 727 obtained 23 September 1974 at 2048 UT
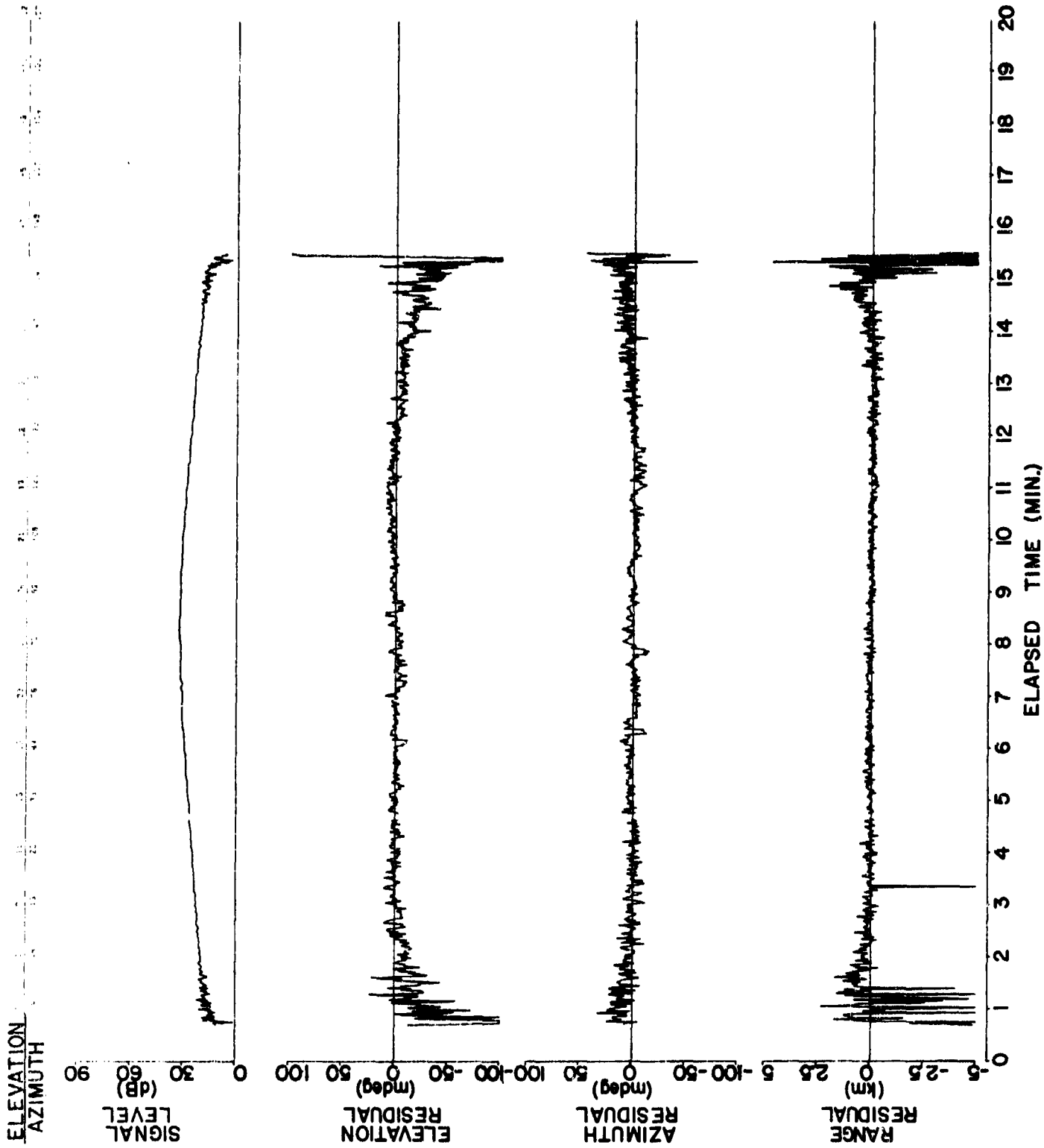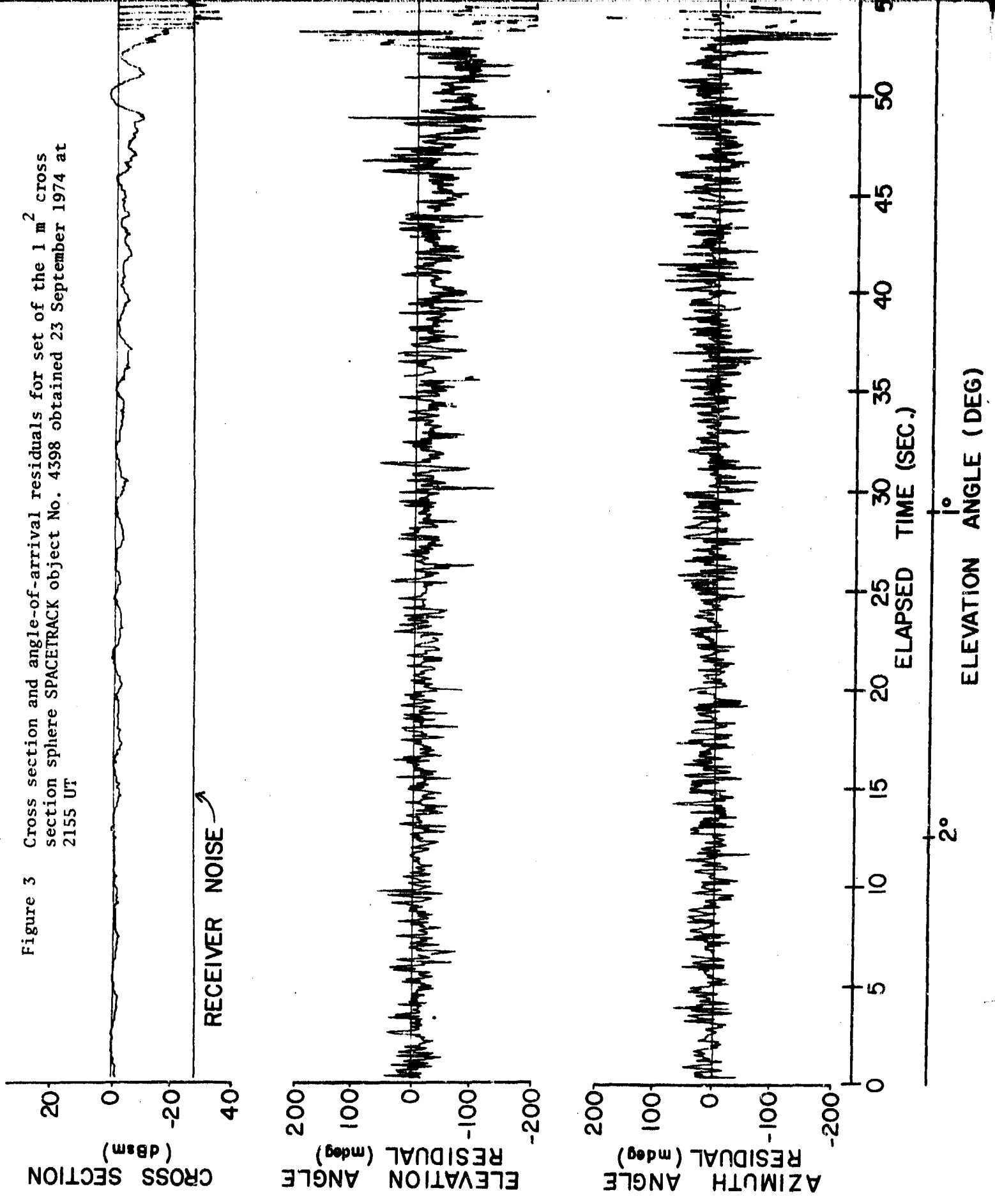
19

Figure 2 CAST summary output data for track of 1 m² cross section sphere SPACETRACK object No. 5398 obtained 23 September 1974 at 2013 UT

20

Figure 3   Cross section and angle-of-arrival residuals for set of the 1 m² cross
section sphere SPACETRACK object No. 4398 obtained 23 September 1974 at
2155 UT

21

20-second smoothing interval, the rms angle-of-arrival fluctuations are reduced by a factor of 4.5 from 30 to 6.7 mdeg.

The rms angle-of-arrival fluctuations for a typical pass of the 1 m^2 cross section sphere are presented in Figure 4. The apparent elevation angle to the sphere is listed on the figure. The rms values are deviations of the raw data from a third degree polynomial fitted to 8.5 seconds of data (128 samples) reported for the midpoint of each interval. Successive data points are for overlapping intervals spaced by 4.3 seconds (64 samples). The rms values at angles between 5° and 40° elevation angle used to derive the reference orbit have rms fluctuations of less than 20 mdeg rms. The 20-second samples therefore have less than a 4.5 mdeg rms fluctuation produced by receiver noise. Over much of a typical arc, the rms values are less than 10 mdeg producing 20-second averages with less than 2 mdeg rms uncertainty. Larger elevation angle fluctuations are apparent at elevation angles above 20° for this particular pass. These are sometimes evident when the antenna moves rapidly in elevation and are generally suppressed when too large by the inverse rms fluctuation weighting and editing employed in ORBFIT.

The rms angle-of-arrival fluctuations for a 0.1 m^2 cross section target are displayed in Figure 5. In this case, the rms fluctuations are larger than for the 1 m^2 sphere for similar observing conditions (range, elevation angle). For this particular sample, the rms fluctuations at a 6° elevation angle are 45 mdeg, three times the observed value for the 1 m^2 cross section sphere (for 0.1 and 1 m^2 spheres at the same range, the ratio should be 3.2), contributing an rms uncertainty of 10 mdeg to the measurement of the 20-second average angle-of-arrival at a 6° elevation angle. At 10° elevation angle, the 0.1 m^2 cross section sphere would contribute 6.7 mdeg rms fluctuation to the 20-second average angle-of-arrival value.

The departure of the elevation angle from the expected (reference orbit) values at low elevation angles is evident in Figure 3. For elapsed times less than 45 seconds, the elevation angle residuals display a relatively smooth trend away from the expected value with the large noise induced fluctuations superimposed on the trend. At five seconds, the average deviation is 8 mdeg; at 40 seconds, the deviation is 24 mdeg. The smoothed deviation represents the uncorrected component
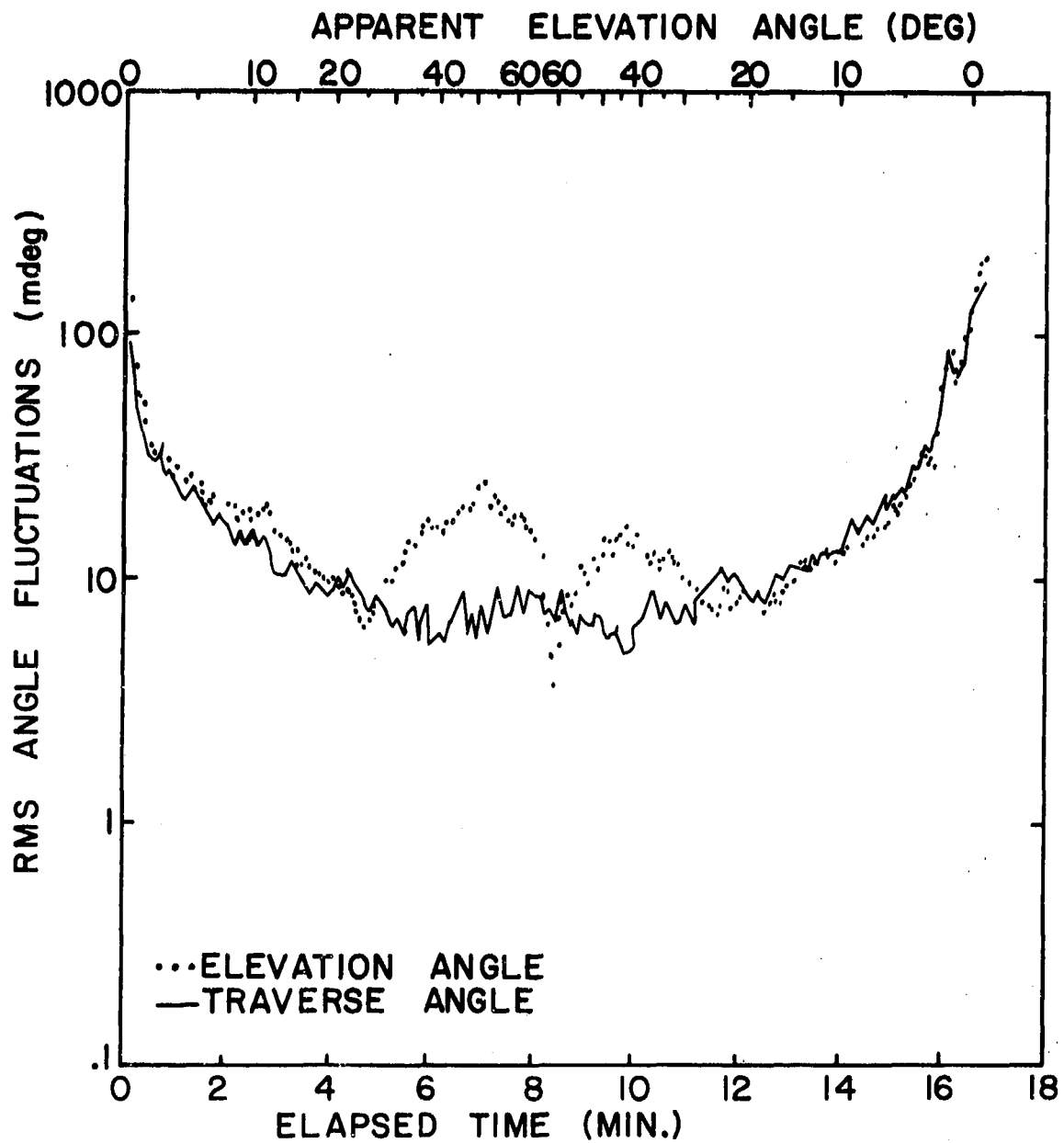
22

Figure 4   RMS angle-of-arrival fluctuations for a high elevation angle
pass of the 1 m² cross section sphere SPACETRACK object No.
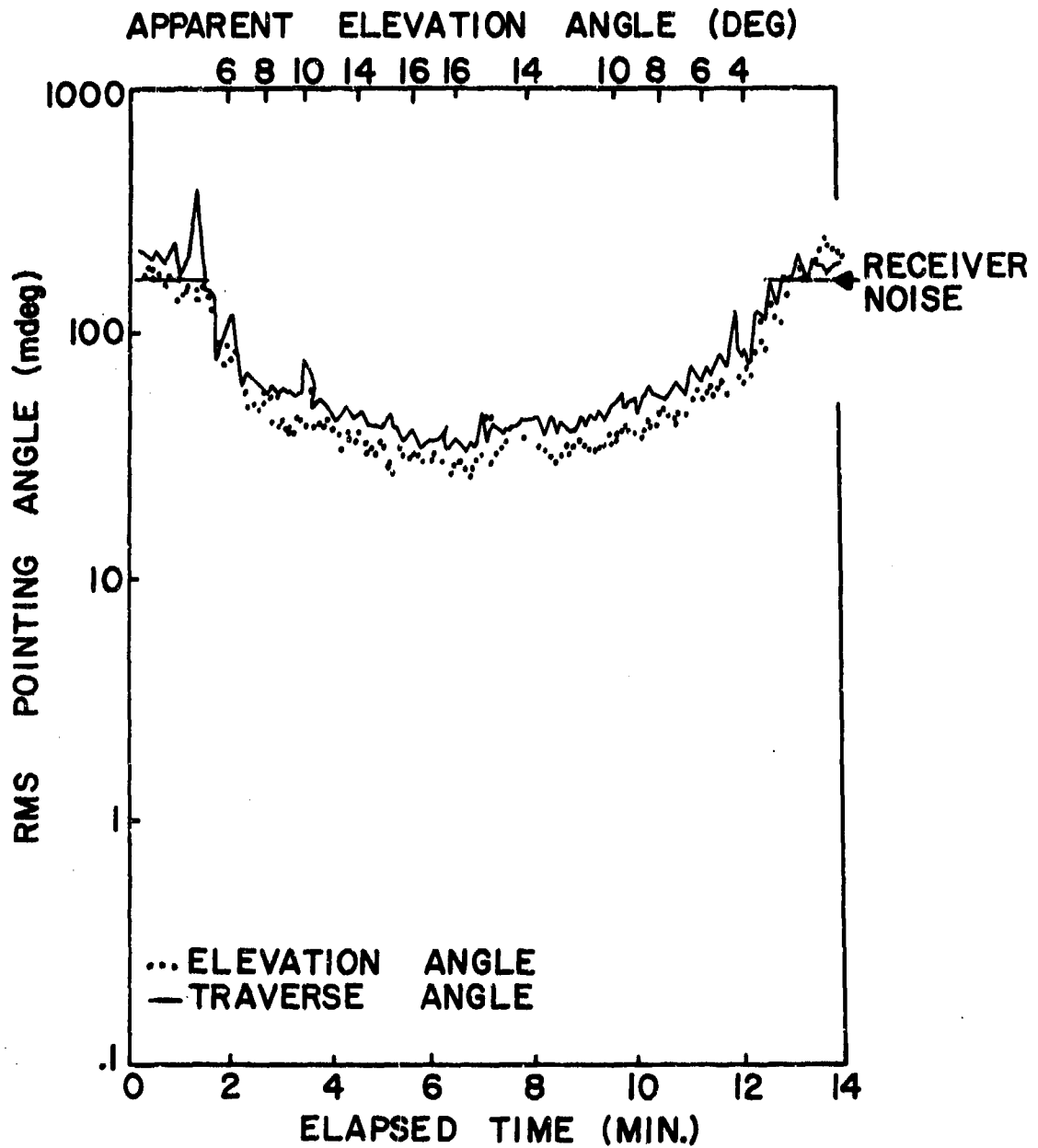5398 obtained 27 August 1974 at 1129 UT

Figure 5   RMS angle-of-arrival fluctuations for a pass of the 0.1 m^2 cross section sphere SPACETRACK object No. 4958 obtained 6 August 1974 at 1143 UT

24

of the bias refraction error, the refraction induced slow departure of the surface refractivity corrected elevation angle values from the reference orbit positions. The 20-second smoothed values provide estimates of the bias refraction effects contaminated by the residual noise fluctuations that remain after averaging and residual noise fluctuations caused by tropospheric angle-of-arrival scintillation.

The data displayed in Figure 3 indicate that the satellite set (disappeared over the local horizon) at about 53 seconds elapsed time. At this time, the cross section value was reduced to the noise level and large random angle-of-arrival values are evident. In the five-second interval prior to set, large amplitude elevation and cross section fluctuations are evident. This behavior is similar to the results reported by Crane (1976b) for the low elevation angle measurements at Haystack. The more extensive instrumentation used for the Haystack observations allowed the identification of these large amplitude fluctuations with internal atmospheric multipath, a refraction induced phenomena, not reflections from the Earth's surface. The relatively large amplitude fluctuations together with the elevation angle fluctuations and lack of azimuth angle fluctuations suggest that these fluctuations are of similar origin.

Cross section observations for the 1 m^2 cross section sphere are depicted in Figures 6 and 7. In these figures, the values are plotted vs apparent elevation angle. The cross section values vary about the expected cross section value of 0.0 dBsm reduced slightly by the effect of atmospheric focusing (the focusing loss is expected to be .6 dB at 3°, see Crane, 1976a; see also next section). The expected cross section values including focusing loss are displayed by the smooth curves on each figure. At the apparent elevation angle values listed on the figure, the one-way gain of the antenna in the direction of the surface is more than 18 dB below the on-axis gain (Crane, 1971) producing a surface reflection caused variation in cross section of less than ±2.5 dB at an apparent elevation angle of 1.3° and of less than ±0.5 dB at a 3° apparent elevation angle. The observed cross section fluctuations are significantly larger being more than 10 dB above the expected value at an apparent elevation angle of 1.06° and 3 dB above the expected value at an apparent elevation angle of 4°. Refractivity disturbed conditions are clearly contributing to these fluctuations.
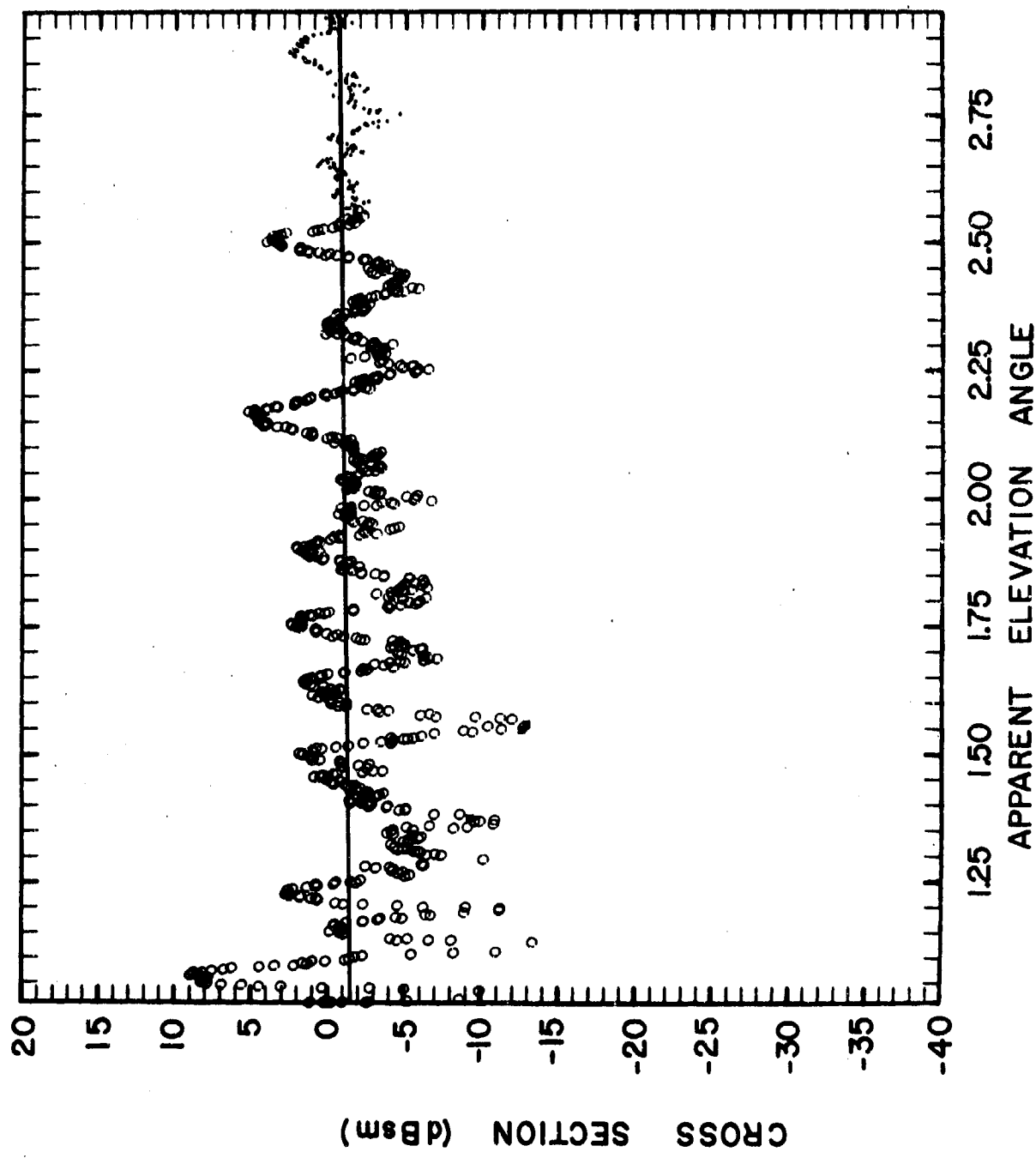
Figure 6   Radar cross section values displayed for each pulse, rise of
1 m² cross section sphere SPACETRACK object No. 4398 obtained
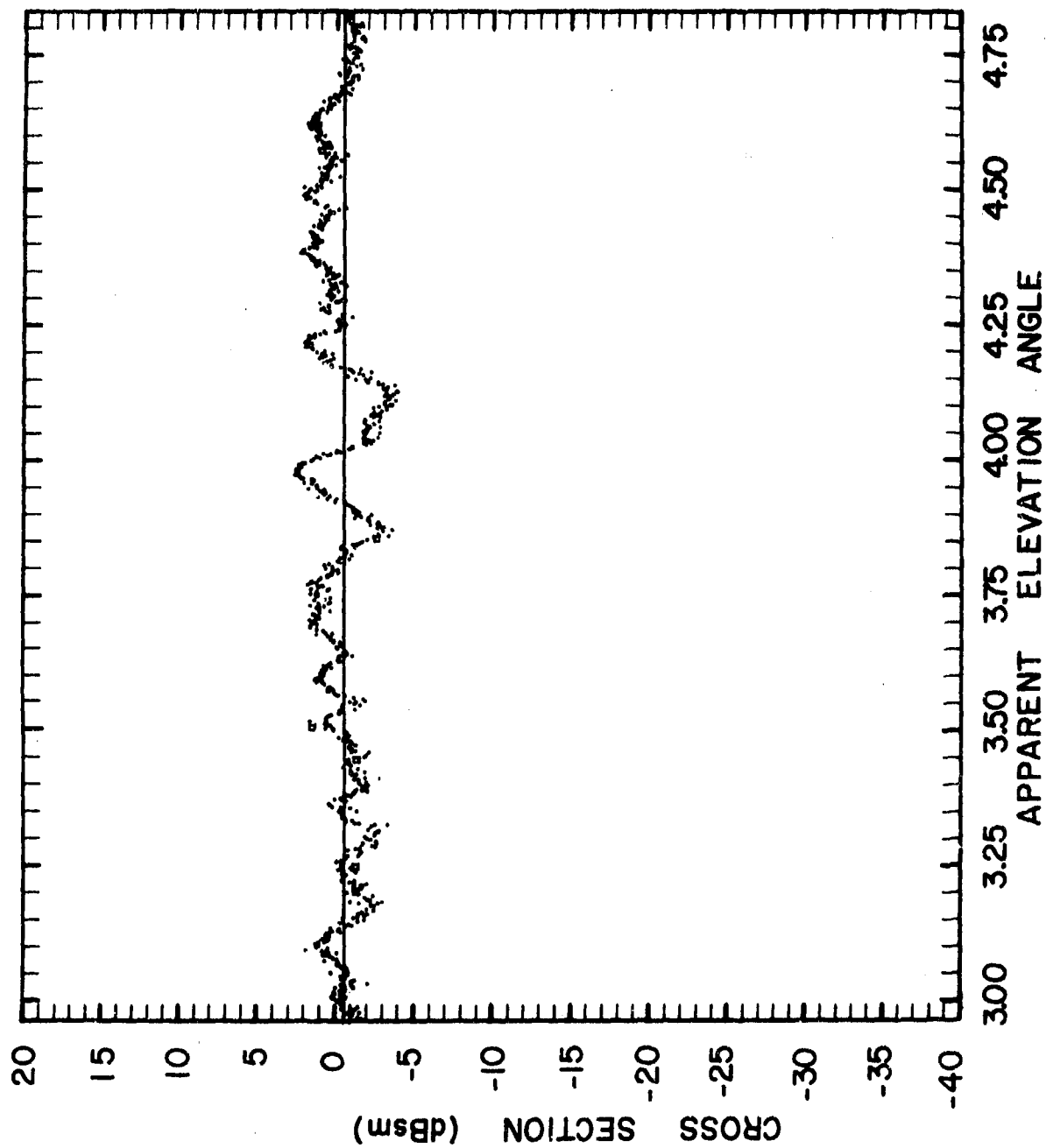27 August 1974 at 0952 UT

Figure 7   Radar cross section values displayed for each pulse, rise of 1 m² cross section sphere SPACETRACK object No. 5398 obtained 27 August 1974 at 0953 UT

The Haystack observations suggest that a monopulse tracker would produce elevation angle error signals that were a significant fraction of the halfpower beamwidth of the antenna in response to internal atmospheric multipath events producing cross section increases in excess of 5-6 dB. From the data in Figures 6 and 7 the time scales of these fluctuations should be of the order of 5 to 10 seconds; the effects of the fluctuations should be reduced to variations of the order of 100 mdeg or less for the Millstone radar system and for a 20-second smoothing interval. The differences between two smoothed samples obtained from the same pass of the 1 m^2 sphere and within a 1° true elevation angle range were as large as 60 mdeg for elevation angles between 1 and 2°, 25 mdeg for elevation angles between 4 and 5°, and 10 mdeg for elevation angles between 9 and 10°. These changes are significantly larger than expected due to signal-to-noise limitations and indicate that the fluctuations are caused by either internal atmospheric multipath or other small scale, large gradient refractive phenomena.

4. RAY-TRACING ANALYSIS

4.1 Ray-Tracing Calculations

The coefficients of the linear relationship between surface refractivity, N_s, and elevation angle error originally provided for use by the joint study and used for elevation angle correction during the 1973-1974 measurement period were derived from ray-tracing calculations using refractive index profiles obtained from radiosonde measurements. The ray-tracing program used for the analysis was developed by the author while at Lincoln Laboratory during the 1966-1968 time period. Since some of the details of the tracing procedure differ from ray-tracing programs developed by others and the program has not been documented elsewhere, it is briefly described in this section.

The equations used for ray-tracing may be obtained from Maxwell's equations (Freehafer, 1951), or from variational principles (Born and Wolf, 1964). From either starting point, the basic equation of geometrical optics, the eikonal equation may be obtained:

$$\nabla S \cdot \nabla S = n^2 \qquad (2)$$

where $S(\underset{\sim}{r})$ = path function, $S(\underset{\sim}{r})$ = constant being the equation of a wavefront, $n(\underset{\sim}{r})$ = index of refraction (assumed to be a real (lossless) scalar, $n = 1 + N \times 10^{-6}$, N = radio refractivity or refractivity). The unit normal to a wavefront (unit vector along the ray) is:

$$\hat{s} = \frac{\nabla S}{n} = \frac{d\underset{\sim}{r}}{ds} \qquad (3)$$

where $\underset{\sim}{r}$ = position vector

s = distance along the ray.

Then

$$\int_{ray} n\, ds = \int_{ray} \nabla S \cdot d\underset{\sim}{r} = S(\underset{\sim}{r}_2) - S(\underset{\sim}{r}_1) = L \qquad (4)$$

where L = path length between points $\underset{\sim}{r}_1$ and $\underset{\sim}{r}_2$ on the ray. Equation (4) provides the basic equation for estimating changes in transit time or electrical path length due to the atmosphere.

The ekional equation may be obtained from equation (4) by requiring
that the path length be stationary along the ray (Fermat's Principle).
The equation for the ray path may be obtained by finding the change in
∇S with distance along the path using equations (2) and (3):

$$\frac{d}{ds} \left(n \frac{d\chi}{ds}\right) = \frac{d}{ds} (\nabla S) = \frac{d\chi}{ds} \cdot \nabla(\nabla S) = \frac{1}{n}\nabla S \cdot \nabla(\nabla S) = \nabla n$$

and the required equation is

$$\frac{d}{ds} \left(n \frac{d\chi}{ds}\right) = \nabla n \tag{5}$$

Equation (5) may be recast as a non-linear coupled set of first order
differential equations for the ray path. Using the following geometrical
relationships to describe the ray trajectory:

$$\frac{dr}{ds} = \sin\alpha \tag{6a}$$

$$\frac{d\Theta}{ds} = \frac{\cos\alpha \, \cos\xi}{r} \tag{6b}$$

$$\frac{d\phi}{ds} = \frac{\cos\alpha \, \sin\xi}{r \, \sin\Theta} \tag{6c}$$

where
α = local elevation angle at r, Θ, ϕ (angle between the tangent
to the ray and its projection in a horizontal plane through
χ),

ξ = local azimuth angle at r, Θ, ϕ (orientation of the projec-
tion of the tangent to the ray in the horizontal plane
measured clockwise from north),

r, Θ, ϕ = point χ on ray trajectory in an Earth centered spherical
coordinate system,

equation (5) becomes

$$\frac{d\alpha}{ds} = \frac{1}{nr} \left[\cos\alpha \, \frac{\partial(nr)}{\partial r} - \sin\alpha \left(\frac{\cos\xi}{r} \, \frac{\partial(nr)}{\partial\Theta} + \frac{\sin\xi}{r \, \sin\Theta} \, \frac{\partial(nr)}{\partial\phi}\right)\right] \tag{6d}$$

$$\frac{d\xi}{ds} = -\frac{1}{nr \, \cos\alpha} \left[\frac{\sin\xi}{r} \, \frac{\partial(nr)}{\partial\Theta} - \frac{\cos\xi}{r \, \sin\Theta} \, \frac{\partial(nr)}{\partial\phi}\right] - \frac{\cos\phi \, \cos\alpha \, \sin\xi}{r \, \sin\Theta} \tag{6e}$$

30

The coupled equations for the ray path must be solved numerically. For special cases, the equations may be considerably simplified. For a horizontally stratified atmosphere, the index of refraction is a function only of the distance from the center of the earth. Equations (6a) to (6e) show that for this condition, the ray trajectory is confined to great circle planes. A first integral of equation (6d) may be performed yielding Snell's Law for a spherically symmetric medium,

$$nr \cos\alpha = K = \text{constant} \tag{7}$$

Equation (7) represents a first order differential equation for the ray path, $\cos\alpha$ being related to the differential change in direction with position along the ray. The spherically symmetric equations may be reduced to quadrature expressions for the path length, path position, and to bending along the ray,

$$\Delta L(h_2, h_1) = L(h_2) - L(h_1) = \int_{r_0+h_1}^{r_0+h_2} \frac{(nr)^2 \, dr}{r\sqrt{(nr)^2 - K^2}} \tag{8}$$

$$\Delta\Theta(h_2, h_1) = \Theta(h_2) - \Theta(h_1) = \int_{r_0+h_1}^{r_0+h_2} \frac{K \, dr}{r\sqrt{(nr)^2 - K^2}} \tag{9}$$

$$\Delta\alpha(h_2, h_1) = \alpha(h_2) - \alpha(h_1) = \int_{(r_0+h_1)n_1}^{(r_0+h_2)n_2} \frac{K \, d(nr)}{(nr)\sqrt{(nr)^2 - K^2}} \tag{10}$$

$$\tau(h_2, h_1) = \Delta\Theta(h_2, h_1) - \Delta\alpha(h_2, h_1) \tag{11}$$

$$\varepsilon(h_2, h_1) = \alpha(h_1) - \tan^{-1}\left[\frac{1}{\tan\Delta[\Theta(h_2, h_1)]} - \frac{(r_0 + h_1)}{\sin[\Delta\Theta(h_2, h_1)](r_0+h_2)}\right] \tag{13}$$

where   L(h) is the electrical path length as given by equation (4) at height h,

Θ(h) is the central angle (earth centered) describing the ray position as shown in Fig. 8 at height h,

α(h) is the local elevation angle at height h

τ(h₂, h₁) is the bending angle or the angle between tangents to the ray at height h_2 and height h_1,
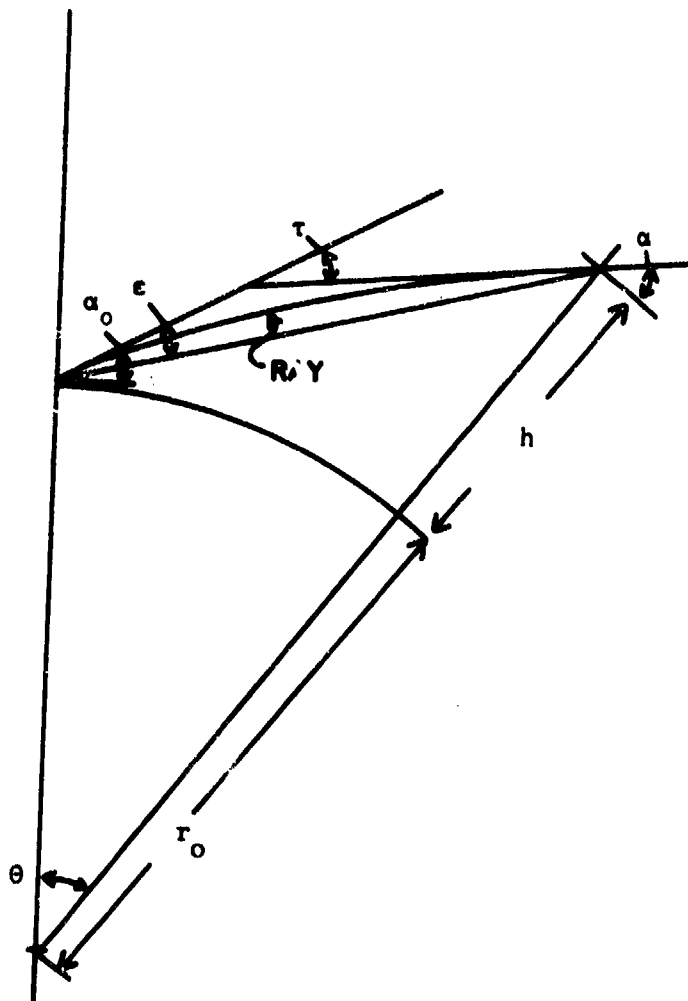
31

Figure 8   Ray path geometry

$\epsilon(h_2, h_1)$ is the elevation angle error or the angle between the ray tangent at h_1 and the actual direction to h_2 from h_1, and

h is the height of the ray above a reference sphere of radius r_o.

The quadrature expressions for the ray may be explicitly determined only when the variation of n with height is specified. For a linear change of n with height, equations (8) to (10) are elliptic integrals. Although elliptic integrals have been tabulated, the changes in L, Θ, and α are too small to effectively use the tables. Alternative approximations also may be used. Explicit evaluation of equations (8) to (10) are possible when the product (nr) is assumed to vary linearly with height. For m - nr, Snell's Law is given by m $\cos\alpha$ = constant and the integrals may be readily evaluated yielding:

$$\Delta\Theta\ (h_2, h_1) = -\frac{K}{\sqrt{w}}\ \log_e \left(\frac{\sqrt{m^2 - K^2} + \sqrt{w}}{r} + \frac{v}{2\sqrt{w}}\right)\Bigg|_{h_1}^{h_2}\ ;\ w > 0$$

$$= \frac{K}{\sqrt{|w|}}\ \sin^{-1}\left(\frac{vr + 2w}{r\sqrt{v^2 - 4\ uw}}\right)\Bigg|_{h_1}^{h_2}\ ;\ w < 0 \tag{13}$$

$$= -\frac{2K}{vr}\ \sqrt{m^2 - K^2}\ \Bigg|_{h_1}^{h_2}\ ;\ w = 0$$

where

$w = b^2 - K^2$

$u = a^2$

$v = 2ab$

and $\qquad$ $m = ar + b$ or $n = a + \dfrac{b}{r}$ between h_1 and h_2;

33

$$\Delta L \ (h_2, h_1) = \sqrt{m^2 - \kappa^2} \ \Bigg|_{h_1}^{h_2} + \frac{b^2}{\kappa} \ \Delta\Theta(h_2, h_1) \ + $$

$$b \ \log_e \ (2ur + v + 2a\sqrt{m^2 - k^2}) \ \Bigg|_{h_1}^{h_2} \ ; \tag{14}$$

and

$$\Delta\alpha \ (h_2, h_1) = \cos^{-1}\left(\frac{K}{m}\right) \ \Bigg|_{h_2}^{h_1} \tag{15}$$

Using the linear change in m approximation, measured index of refraction profiles (functions of height) may be approximated by a number of layers each with linear changes in m and rays are traced through the layers using equations (13) to (15). This process is significantly faster than numerically integrating the original ray equations. Index of refraction profiles for use in estimating the effects of atmospheric refraction are generally obtained from radiosonde balloon flights and are available only as tables of radio refractivity $N = (n - 1) \times 10^6$ and height. The variation in n between the reported levels is not provided. The linear m approximation allows rapid computation of the ray trajectory given the tabulated values. The tracing program package developed at Lincoln Laboratory could perform either the rapid linear m profile calculations or the slower numerical integrations. Comparison between computations made using the linear m approximation and numerical tracing using equations (6a) to (6e) shows the errors to be small fractions of a percent, significantly smaller than the errors due to an imprecise knowledge of the profile.

The ray position $\Theta(h)$; path length, $L(h)$; and bending $\tau(h_2, h_1)$ are parameters that describe the trajectory of a ray in space. The variation in intensity (magnitude of the time averaged Poynting vector) may also be computed using geometric optics. Since the direction of the ray, $\hat{s}$, is the direction of energy propagation or of the Poynting vector in a scalar medium, the principle of conservation of energy requires that

34

$$\nabla \cdot (I\hat{s}) = 0$$

where I = intensity.

Therefore, the intensity is proportional to the area of a wavefront enclosed in a narrow bundle or tube of rays. For the case of a horizontally homogeneous atmosphere, the focusing factor or ratio of computed intensity to intensity for free space propagation to the same distance may be given by a quadrature formula and, for a horizontally homogeneous atmosphere, by an explicit relationship similar to those for ΔL, $\Delta\Theta$, and $\Delta\alpha$:

$$\frac{I(h_2)}{I_f(h_2)} = F(h_2) = \frac{S(h_2)\cos^2(\alpha(h_o))}{r^2 \sin(\alpha(h_o)) \sin(\Delta\Theta(h_2,h_o)) D(h_2,h_o)} \tag{16}$$

where
$$D(h_2,h_o) = \sin(\alpha(h_2)) \left[\Delta\Theta(h_2,h_o) + \int_{r_o+h_o}^{r_o+h_2} \frac{K^3 \, dr}{r[m^2 - K^2]^{3/2}} \right]$$

$I_f(h_2)$ is the intensity for free space propagation and

S is distance along the ray from h_o to h_2; h_o is the initial ray height.

The effect of extinction by atmospheric gases or condensed water (cloud particles or hydrometeors) along the ray path may be included in the evaluation of intensity by computing the line integral of the extinction cross section per unit volume along the ray:

$$I = F(h_2) \, I_f e^{-\int_0^{S(h_2)} \beta ds} \tag{17}$$

where $\int_0^{S(h_2)} \beta ds$ is the line integral of β, the extinction cross section per unit volume along the path.

For a horizontally homogeneous atmosphere, the line integral of β is given by:

$$\int_0^{S(h_2)} \beta(s)ds = \int_{r_o+h_1}^{r_o+h_2} \frac{\beta(r)m dr}{\sqrt{m^2 - K^2}} \tag{18}$$

35

4.2 Simulation of Refraction Effects

The refraction effects calculated by the ray-tracing program are position errors, bending values, and attenuation due to focusing. A set of sample calculations are given in Table 4. The geometric parameters h, α, ϑ and the derived parameters L, ΔL, ε, τ and F are listed. The central angle, Θ, is tabulated as surface distance which is defined as $r_o\Theta$. The starting height was 156 m, the height of the phase center of the Millstone Hill L-band antenna above mean sea level. The 25 km height is the top of a typical profile, 1000 km the height of the orbiting spheres, and 6371 km is one earth radius.

The ray tracings listed in Table 4 were calculated using the radiosonde data for heights below 30 km; the January, 45°N latitude U.S. Standard Atmosphere (ESSA, 1966) for heights between 50 and 100 km; and zero radio refractivity above (N = 0; n = 1). The profiles were smoothly connected and ionospheric effects were ignored. The sample calculations show that the bending values are within 99 percent of the value for a 1000 km height by a height of 25 km at an apparent elevation angle (α) of 1° (5 mdeg difference) and are within 97 percent of the value for a 1000 km height by a height of 25 km at an apparent elevation angle of 10°. The elevation angle errors change more slowly; the differences between elevation angle error and bending (elevation angle error at an infinite height) are 4 percent (19 mdeg) at a 1000 km height and an apparent elevation angle of 1° and 2 percent (4 mdeg) at the same height and a 10° elevation angle. The range errors increase rapidly at low heights but only very slowly at heights above 100 km. The slow change at heights above the region for which N is zero is caused by the change in curved path geometry, not the change in refractive index along the path. Focusing losses also continue to change at higher altitudes due to the change in curved path geometry. For radar applications (two way propagation) twice the focusing loss value should be used.

To simulate refraction errors for the Millstone Hill L-band radar system, a number of ray tracings were performed using data from the nearest radiosonde station with a similar climate. Data from Albany, New York were used for the analysis. Although the radiosonde station at Portland, Maine is closer, it was not used because of its proximity to

TABLE 4

SAMPLE RAY TRACING
Portland, Maine Radiosonde Sounding, 17 February 1969, 00 UT, N_s = 304.2

h Height (km)	α Elevation Angle (deg)	θ Surface Distance (km)	L Range (km)	ΔL Range Error (m)	ε Elevation Error (mdeg)	τ Elevation Bending (mdeg)	F Focusing Loss (dB)
0.156	1.000						
10.0	3.124	277.34	277.77	54.45	216.15	369.60	0.13
25.0	4.961	489.63	491.17	63.33	304.00	442.08	0.28
100.0	10.030	1053.9	1065.66	65.01	380.68	446.95	0.45
1000.0	30.176	3294.0	3643.77	65.58	427.57	446.95	0.55
6371.2	59.994	6609.8	10973.22	65.66	440.52	446.95	0.58
0.156	2.000						
10.0	3.572	203.83	204.26	38.01	154.05	260.98	0.07
25.0	5.254	398.15	399.69	45.70	227.88	326.45	0.17
100.0	10.177	946.12	957.92	46.90	287.63	331.10	0.29
1000.0	30.221	3175.0	3524.69	47.10	313.69	331.10	0.35
6371.2	60.009	6487.4	10850.82	47.16	327.26	331.10	0.37
0.156	3.000						
10.0	4.212	156.83	157.29	28.55	116.52	196.65	0.04
25.0	5.709	329.49	331.07	35.16	178.86	253.98	0.11
100.0	10.418	853.55	865.41	36.13	227.53	258.32	0.20
1000.0	30.296	3064.0	3413.80	36.22	250.52	258.32	0.23
6371.2	60.035	6370.9	10734.41	36.25	255.84	258.32	0.24
0.156	5.000						
10.0	5.809	104.20	104.77	18.63	76.28	128.39	0.02
25.0	6.968	237.96	239.73	23.59	122.14	171.86	0.06
100.0	11.152	703.60	715.77	24.31	157.29	175.52	0.10
1000.0	30.534	2858.9	3209.13	24.34	171.46	175.52	0.12
6371.2	60.115	6148.3	10512.23	24.35	174.28	175.52	0.12
0.156	10.000						
10.0	10.425	54.63	55.57	9.77	39.64	66.63	0.01
25.0	11.107	133.34	135.90	12.63	65.61	91.67	0.02
100.0	14.093	465.55	479.62	13.08	85.76	94.06	0.03
1000.0	31.627	2415.3	2769.29	13.09	92.63	94.06	0.04
6371.2	60.491	5625.0	9993.39	13.09	93.67	94.06	0.04
0.156	20.000						
10.0	20.209	26.88	28.65	5.02	19.45	32.68	0.00
25.0	20.558	67.14	71.72	6.54	32.56	45.39	0.01
100.0	22.261	256.56	277.16	6.79	42.89	46.67	0.01
1000.0	35.662	1746.7	2123.14	6.79	46.18	46.47	0.01
6371.2	61.966	4671.7	9073.09	6.79	46.56	46.67	0.01

the coast. A sample of 273 soundings from the months of February and August for the years 1966, 1967 and 1968 were used. Every 00 and 12 UT sounding from each month was traced, but only 273 soundings reached a height of 25 km. Scattergrams of bending values versus reported surface refractivity are depicted in Figures 9 and 10 for apparent elevation angles of 1 and 10 degrees, respectively.

4.3 Surface Correction Model

The bending values to a height of 25 km were used to model the elevation angle errors to be expected in observing satellites at altitudes above 1000 km. As evident in Table 4, the bending values at a height of 25 km are a few percent lower than the values for heights above 100 km but the elevation angle errors are also a few percent lower than the bending values for heights above 1000 km. At elevation angles above 5°, the elevation angle error at a height of 1000 km is within 1 mdeg of the bending value at a height of 25 km. Since the expected rms fluctuations of bending (or elevation angle) is larger than 2 mdeg for apparent elevation angles less than 5° increasing to a value of 12 mdeg at 1° when surface correction is used, a more complex height dependent elevation angle error correction model was not considered and the easier to apply bending correction model was used for the estimation of refraction effects.

A linear regression analysis was performed on the bending-to-25-km-height values and their associated surface refractivity values. Ray tracing calculations were performed at apparent elevation angles of 0.1, 0.2, 0.5, 1.0, 2.0, 3.0, 5.0, 10.0, 20.0 and 50.0 degrees for use in the regression analysis. The result is a set of regression coefficients for each apparent elevation angle. Logarithmic interpolation was used to provide coefficients at 0.5° apparent elevation steps for angles below 6°, 2° steps for angles between 6 and 20° and 10° steps above 20°. Linear interpolation was used to provide the coefficients for the apparent elevation angle of the data to be processed by CAST or ORBFIT. Table 5 presents the results of the regression analysis; Table 6 provides the interpolated coefficients used in the computer correction of elevation angle error.
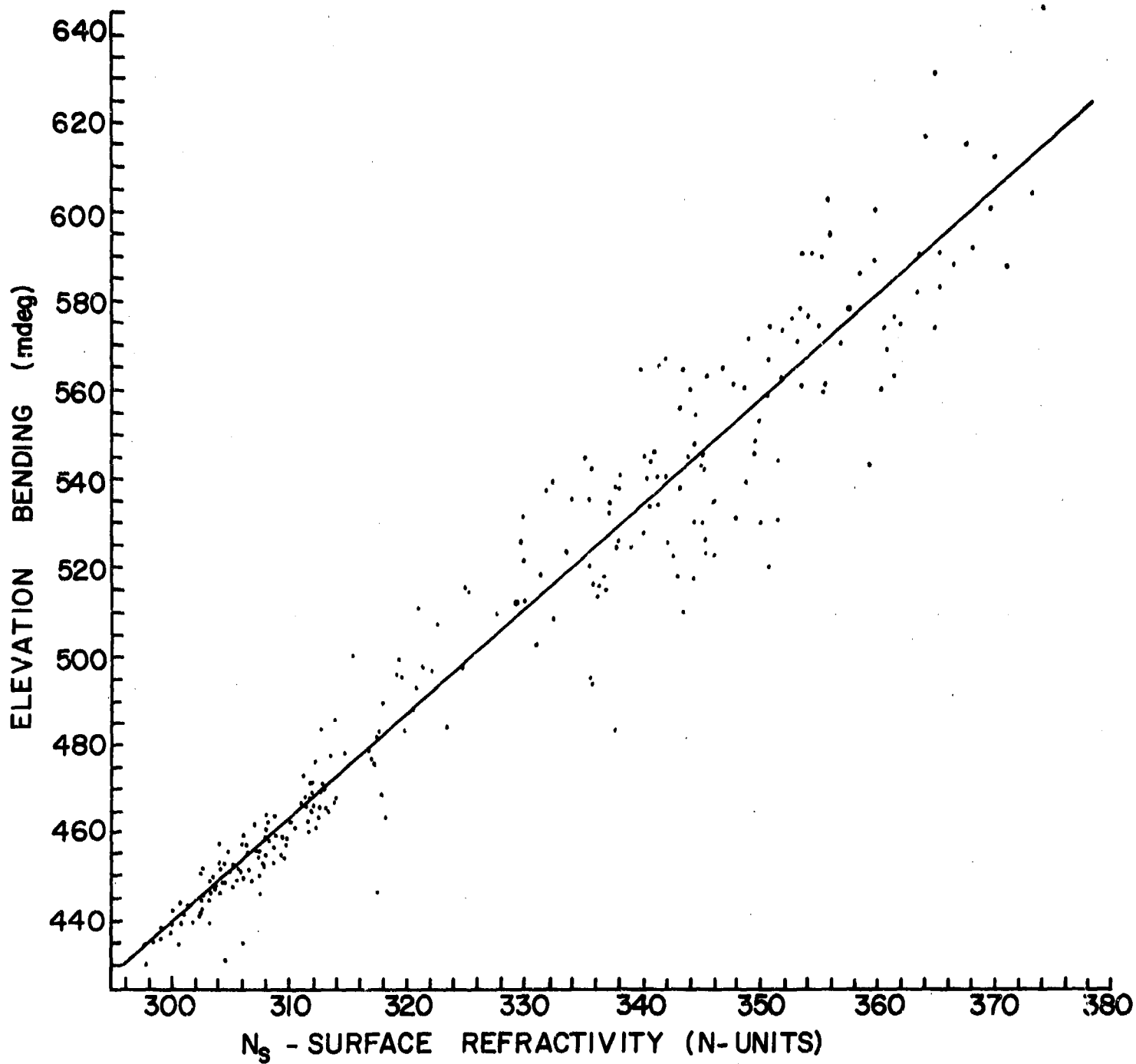
Figure 9   Simulated elevation bending vs surface refractivity for
            tracings to a height of 25 km and an apparent elevation angle
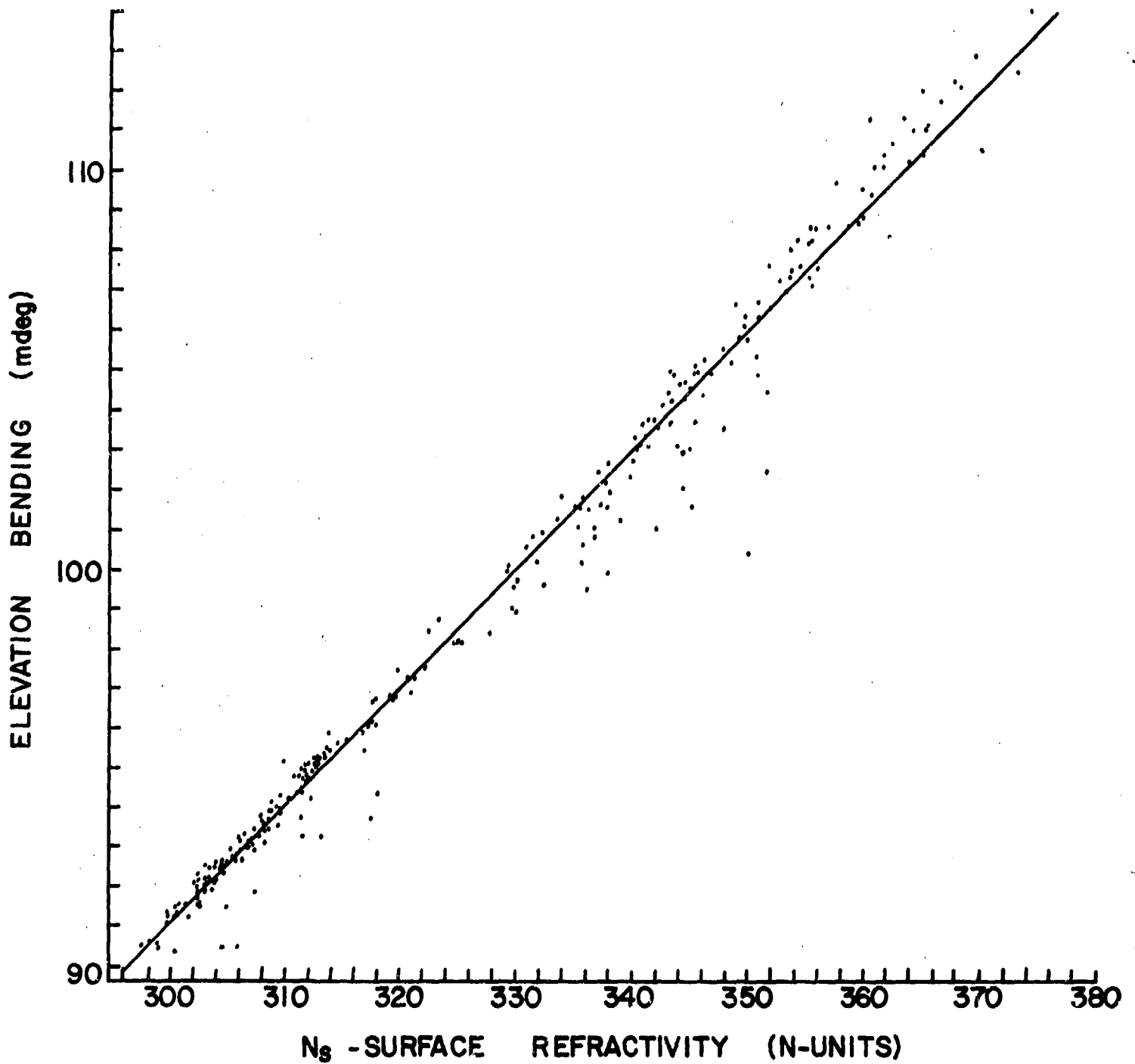   of 1 degree, Albany data set

Figure 10 Simulated elevation bending vs surface refractivity for
tracings to a height of 25 km and an apparent elevation angle
of 10 degrees, Albany data set

TABLE 5

REGRESSION COEFFICIENTS

Apparent Elevation Angle (deg)	Regression Coefficients* A (mdeg)	B (mdeg/N)	Residual Error After Correction (mdeg)	Correlation Coefficient	Mean Bending (no correction) (mdeg)	RMS Deviation About Mean (no correction) (mdeg)
0.1	-1112.8	5.778	89.3	0.81	772.6	152.0
0.2	-889.2	4.951	63.9	0.85	727.6	123.0
0.5	-512.3	3.473	26.5	0.94	622.2	78.3
1.0	-268.3	2.372	12.3	0.97	506.4	51.9
2.0	-95.91	1.4094	5.0	0.99	364.5	30.4
3.0	-40.98	0.9854	3.1	0.99	280.9	21.2
5.0	-10.232	0.9096	1.9	0.99	188.9	13.1
10.0	-0.305	0.3086	0.99	0.99	100.5	6.6
20.0	0.565	0.1505	0.49	0.99	49.7	3.2
50.0	0.237	0.0461	0.15	0.99	15.3	1.0

*$\varepsilon \approx \tau = A + BN_s$ (mdeg)

Surface refractivity: Mean = 326.6
RMS deviation about mean = 21.2

TABLE 6

CORRECTION MODEL

$$\varepsilon = A + BN_s; \quad A = A_i + \left(\frac{A_{i+1} - A_i}{e_{i+1} - e_i}\right) \cdot (E - e_i)$$

$$B = B_i + \left(\frac{B_{i+1} - B_i}{e_{i+1} - e_i}\right) \cdot (E - e_i)$$

i	Apparent Elevation Angle (deg) e_i	Regression Coefficients (mdeg) A_i	(mdeg/N) B_i
1	0	-1210.0	6.25
2	.5	-512.3	3.47
3	1	-268.3	2.37
4	1.5	-160.0	1.78
5	2	-95.9	1.41
6	2.5	-57.0	1.16
7	3	-41.0	0.98
8	3.5	-29.0	0.87
9	4	-20.5	0.77
10	4.5	-14.2	0.68
11	5	-10.2	0.609
12	5.5	-7.1	0.555
13	6	-5.0	0.511
14	8	-1.26	0.386
15	10	-0.305	0.308
16	12	-0.131	0.256
17	14	+0.048	0.218
18	16	+0.217	0.190
19	18	+0.319	0.168
20	20	+0.565	0.151

5. ANALYSIS OF REFRACTION MEASUREMENTS

5.1 Elevation Angle Error Observations

Radar observations of spheres obtained during the last two tracking sessions, 9-14 September and 23-28 September 1974, were analyzed for refraction effects. These data represent the best data from the 1973-1974 measurement period having both the most accurate calibration coefficients and the most refined observing techniques. The surface refractivity values for each tracking session are displayed in Figures 11 and 12. The refractivity data were smoothed for 1000 samples before recording. The variations of surface refractivity over the eight days of observation nearly span the variation encountered in the Albany data set. The diurnal variation in N_s is clearly evident in the data as well as longer term trends.

The smoothed, corrected radar observations were compared with the ORBFIT reference orbits. The resulting angle-of-arrival differences, the residual elevation angle errors, were tabulated in $1°$ true elevation angle intervals. Although refraction effects may vary rapidly over elevation angle intervals as small as $1°$ at low elevation angles, the $1°$ steps were used for analysis since the major elevation angle dependence had been removed using the surface refraction correction model. The tabulated values for all sphere passes are displayed for selected elevation angles in Figures 13-15. The lines displayed on each figure are the results of a regression analysis of residual error vs. N_s. In each case (see Table 1) the correlation coefficient for the residual error vs. N_s was not significantly different from zero (all but one case at the 1σ level, no cases at a lower significance level). The lack of correlation implies that the surface correction procedure using the apriori simulation results removed all the variance associated with N_s; no further improvement is possible using a linear relationship between elevation angle error and N_s.

The observed residual elevation errors are not correlated; therefore, the refraction correction procedure can be worked backwards to provide estimated of the total, uncorrected refraction error. The results of this operation are displayed in Figure 16 and are listed in
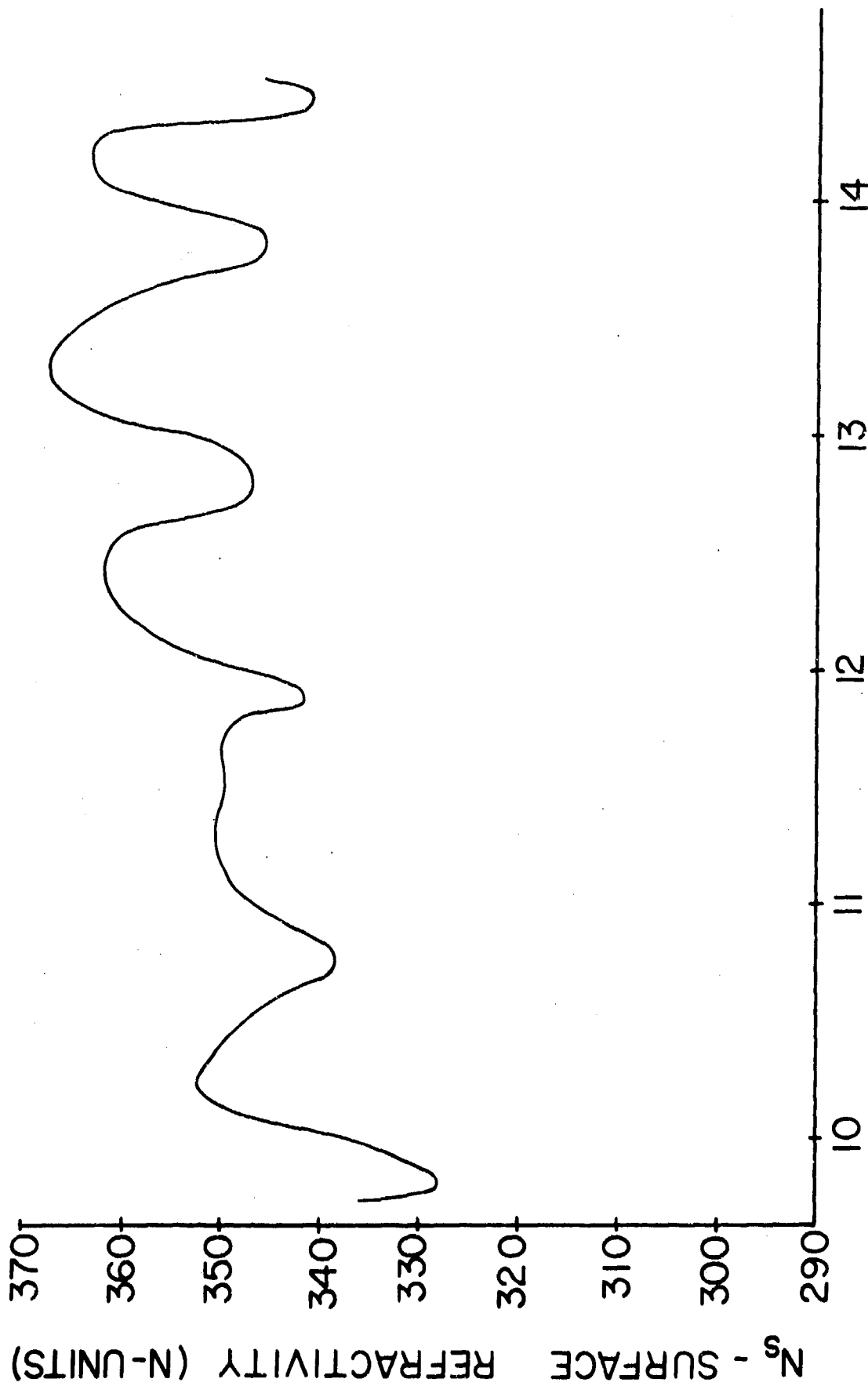
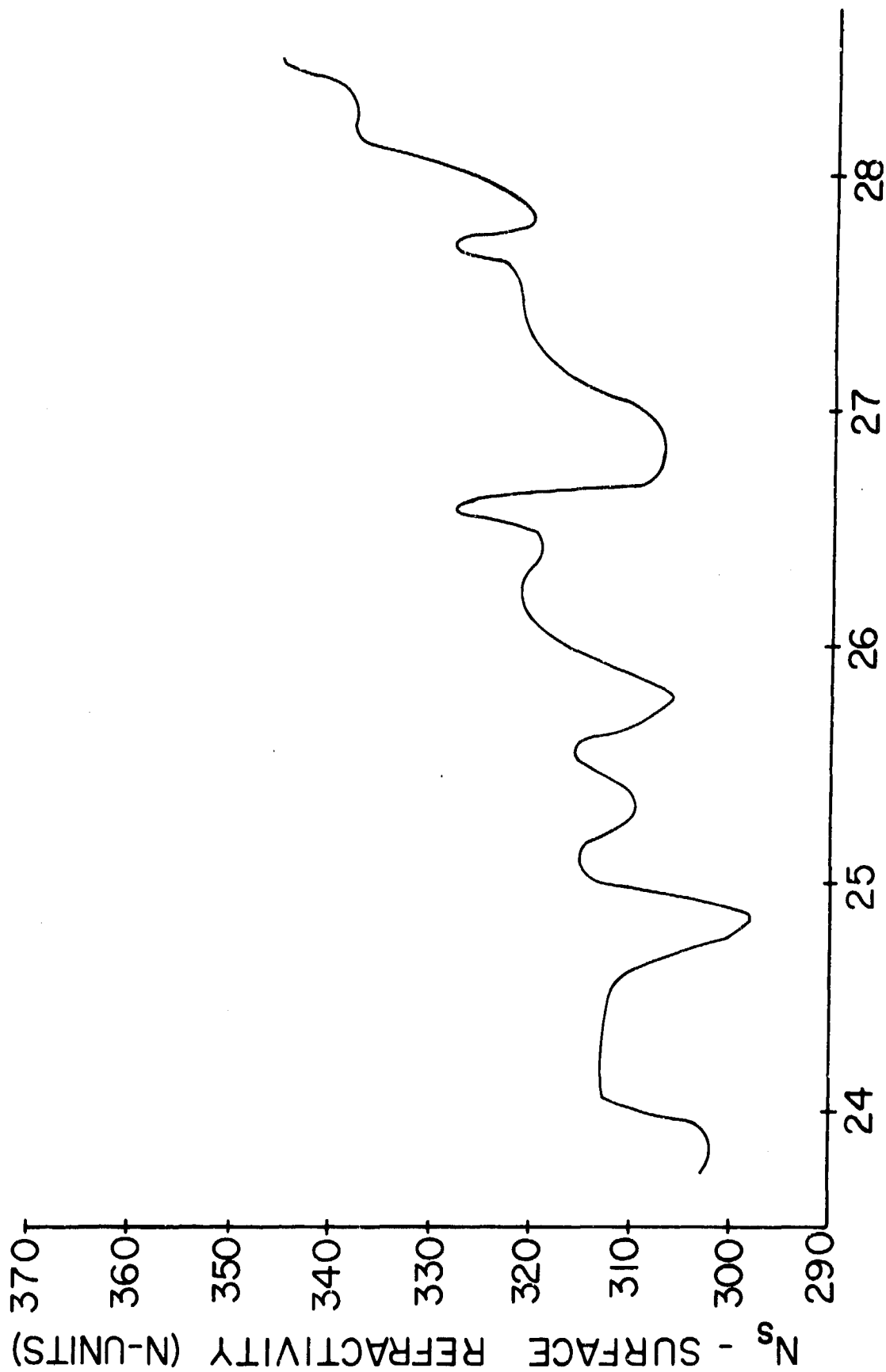Figure 11 Surface refractivity 10-14 September 1974 tracking session

44

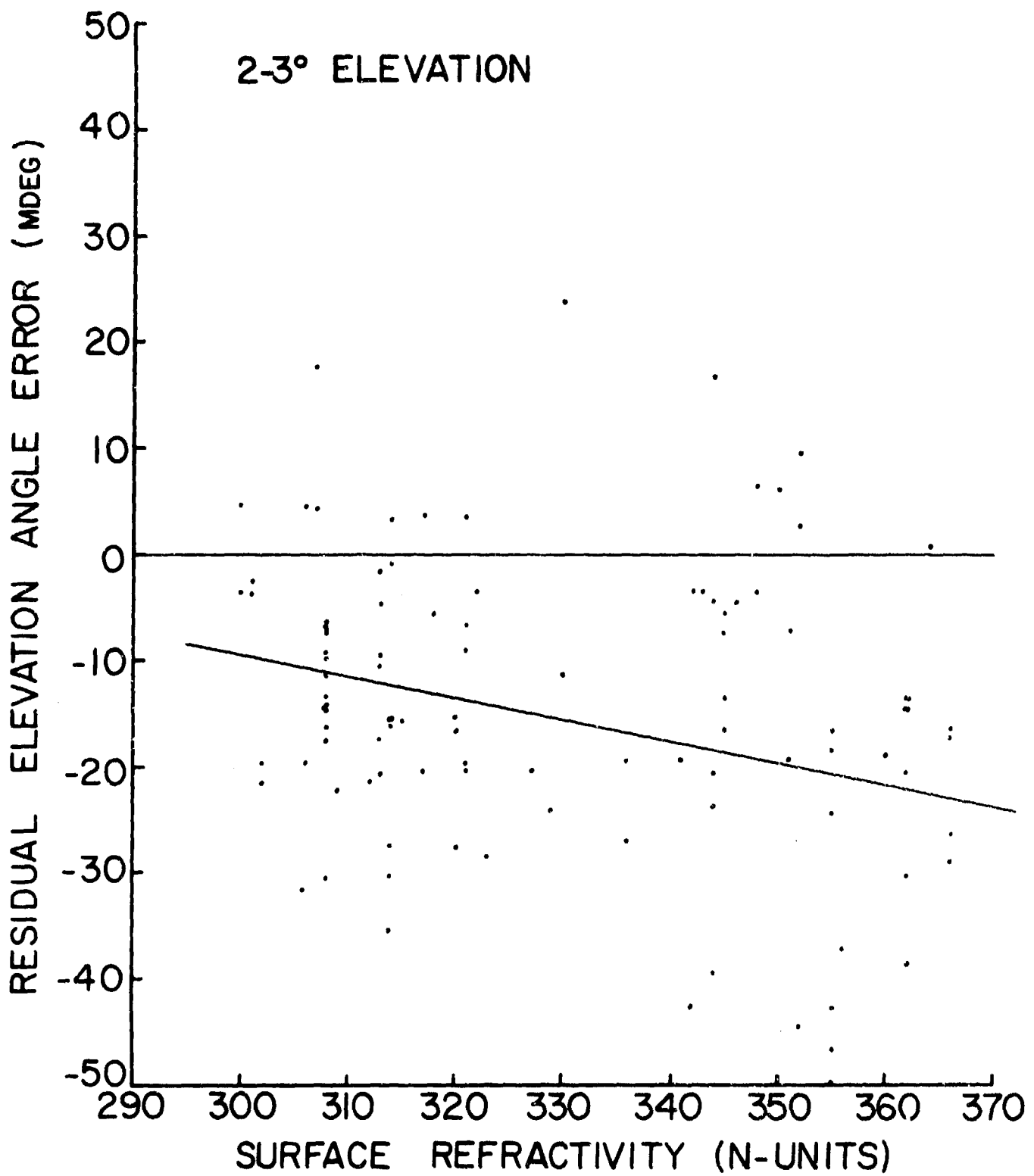Figure 12 Surface refractivity 24-28 September 1974 tracking session

45

Figure 13   Residual elevation angle errors, 2-3° true elevation angle
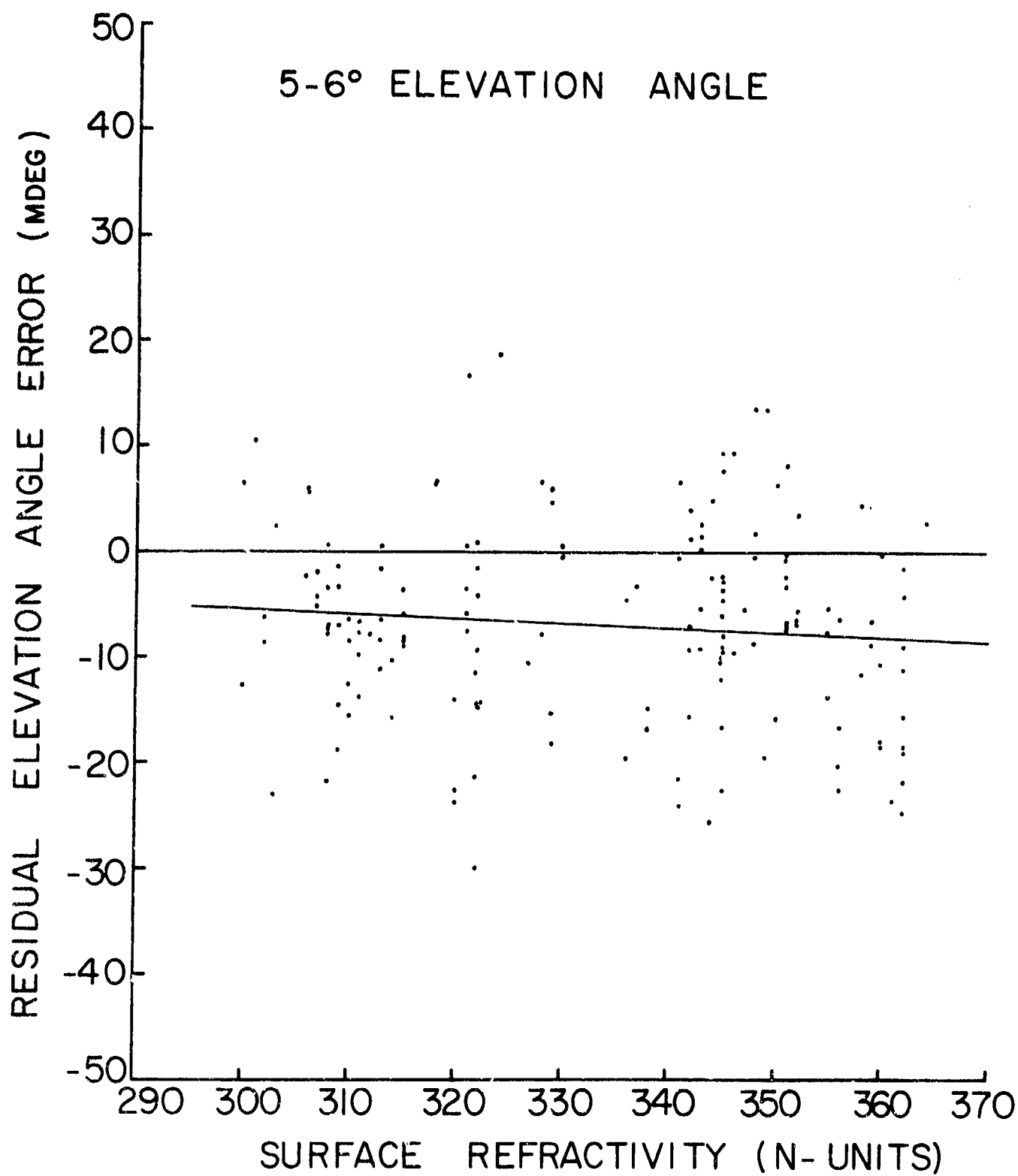interval

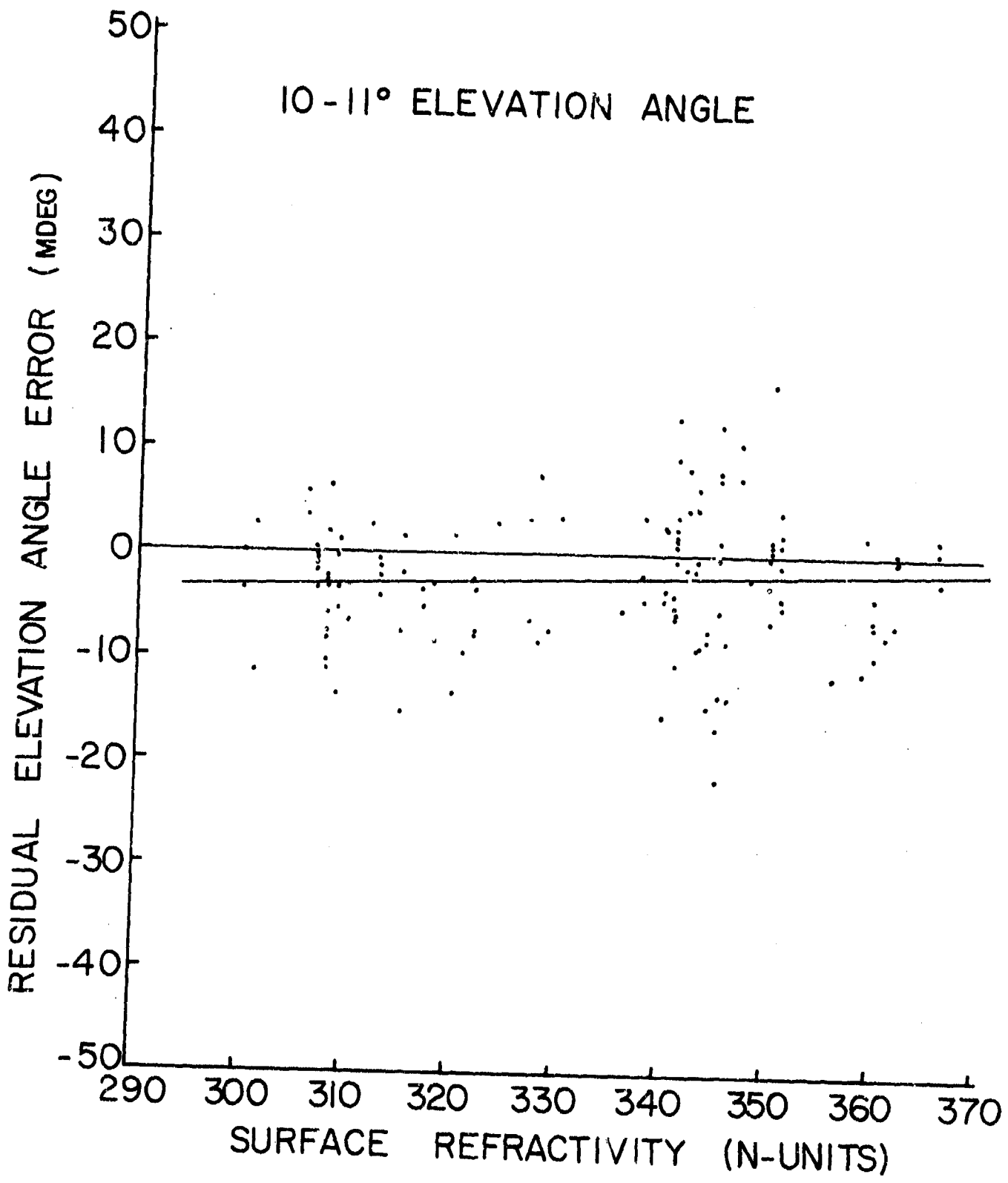Figure 14   Residual elevation angle errors, 5-6° true elevation angle
        interval

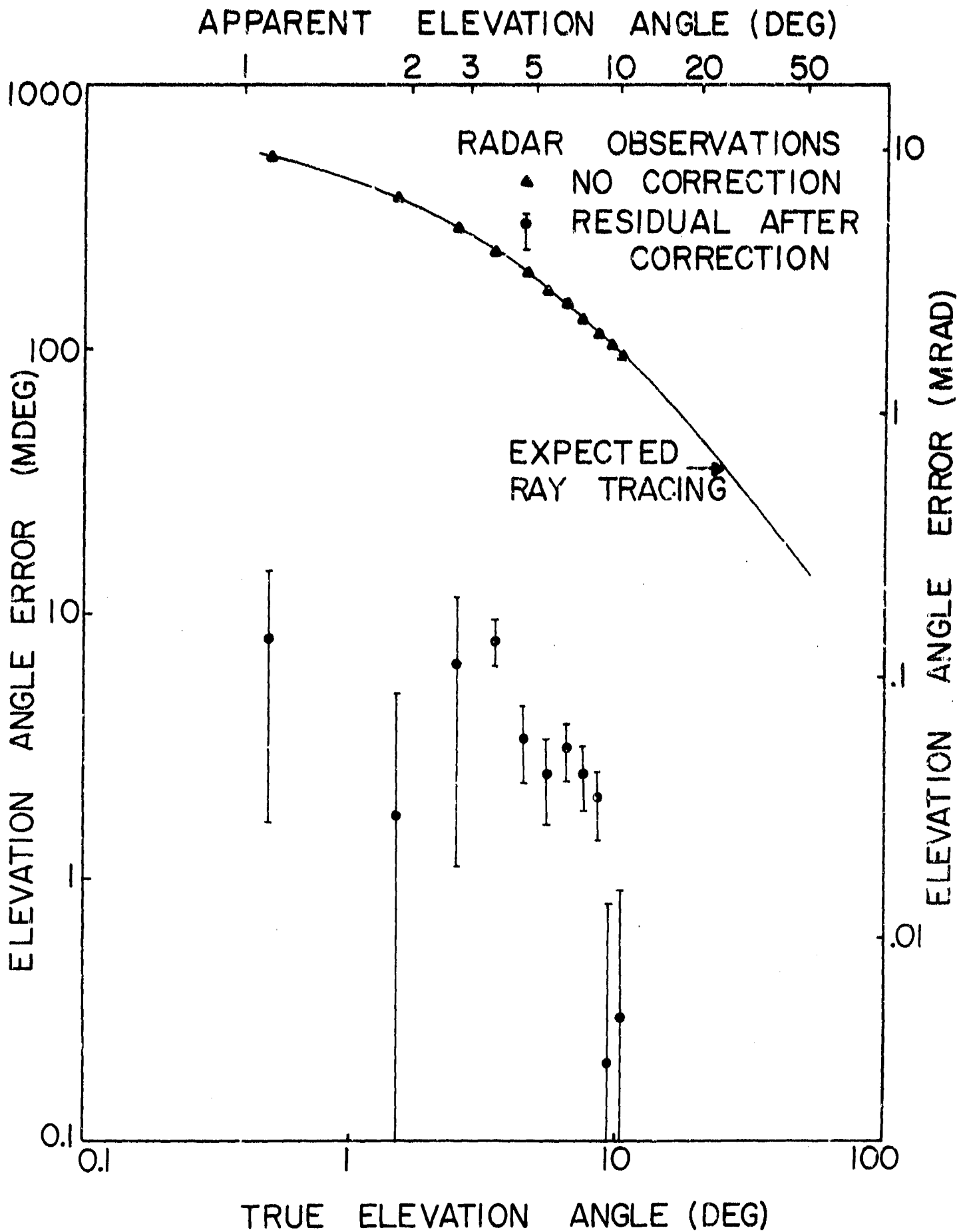Figure 15   Residual elevation angle errors, 10-11° true elevation angle
interval

48

Figure 16 Comparison between averaged simulated or expected and averaged
observed refraction effects

49

Table 1. The elevation angle residuals were averaged for each true
elevation angle analysis interval. The bending correction was then
removed to provide estimates of the mean elevation angle error.
These are plotted as radar observations; no correction. The mean bending
values calculated at a height of 25 km were then approximately adjusted
to estimate the elevation angle error at 1000 km height. This adjustment
was accomplished by calculating the difference between bending error
and elevation angle at a height of 1000 km and a surface refractivity
value corresponding to the mean N_s value in each elevation analysis inter-
val (see Table 1). Adjustment was not made for the differences between
bonding calculated to a height of 25 km and bending calculated to a height
of 1000 km.

The results of the comparison between the expected (simulated
adjusted to elevation angle error) and observed elevation angle errors
are displayed in Figure 16 and Table 1. The differences between the two
refraction effects are listed together with error bounds to represent
the effects of observed fluctuations. At true elevation angles below 2°,
the refraction correction was underestimated, above 2° the correction
was oversestimated. At 10° elevation angle, the difference between
bending to 25 km and bending to 1000 km height should be the order of
3 mdg suggesting that although near perfect agreement is shown at these
elevation angles, the residual uncertainty is closer to 3 mdeg. This
larger value is reasonable considering the residual uncertainties in
system calibration, the orbit determination program and the neglect of
other phenomena such as ionospheric bias refraction. The latter effect,
although relatively small, at 1295 MHz (L-band) still can contribute as
much as 2 mdeg increase in elevation angle error in the elevation angle
range of interest at local noon. In the evening, ionospheric bias
refraction contributes less than 0.3 mdeg. At lower elevation angles,
the simulated values tend to be too large in the 3-5° true elevation
angle range but not by a significant amount. For elevation angles below
2°, the differences between the measured and simulated refraction errors
are reduced to near zero when the additional correction for bending
above a 25 km height are included. In general, the observed and simula-
ted mean refraction errors agree within the approximately 3 mdeg measure-
ment error of the Millstone L-band radar system.

5.2 Residual Errors After Correction

On average, the residual errors after correction are zero; the dif-
ferences between the observed and expected values were smaller than the
overall measurement uncertainty of the Millstone L-band radar. The same
zero average residual error would have been accomplished if the average
refraction error was used for correction rather than the more complex
surface correction procedure. The test of the surface correction pro-
cedure is the measurement of the reduction in variance of the residual
error associated with the use of the correction procedure. Again, since
the residual errors after correction were not correlated with N_s, the
reduction in variance (or in rms deviation about the mean or correction
estimate) could be estimated. The residual receiver noise induced ele-
vation angle fluctuations, however, were relatively large and the effects
of receiver noise were modeled prior to estimating the reduction in
variance.

The sample observations described in Section 3.4 showed that the
receiver noise caused angle-of-arrival measurement fluctuations were
sphere size (signal-to-noise) dependent. The effect of receiver noise
plus the statistical errors in orbit fitting were reduced by processing
the data by sphere cross section value and subtracting the variance
estimated for receiver noise plus orbit fitting uncertainty from the
variance of the observed residuals. Since insufficient statistical
information was available to do the noise subtraction by satellite,
range, cross section, and elevation angle, a composite method was used.
The variance data were tabulated by elevation angle interval and satel-
lite cross section value. The residual fluctuations about the reference
orbit at elevation angles between 5° and 40° were used as an estimate of
the composite noise, receiver noise and orbit fit uncertainties, and the
mean square residual value was subtracted from the tabulated value for
each elevation angle increment. The rms noise values were 6.0 mdeg for
the 1 m^2 target, 6.8 mdeg for 0.2 m^2 targets and 7.4 mdeg for the 0.1 m^2
target. The resultant rms deviations about the surface corrected values
are displayed in Figure 17. The data are displayed by sphere cross
section and a composite value for all the sphere measurements is provided
which was calculated by summing the noise corrected variances. The dif-
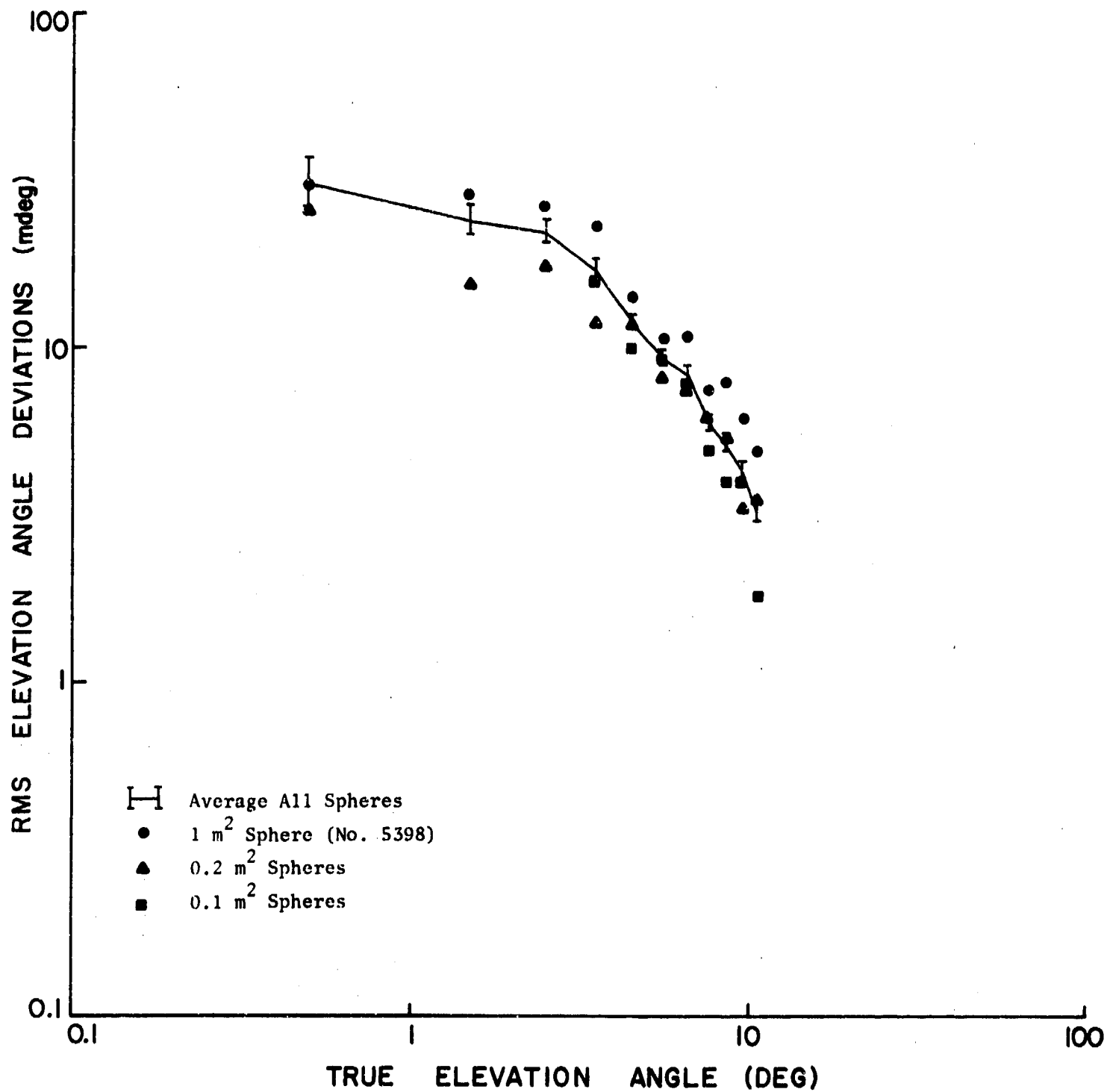ferences between the variance estimates at elevation angles above 8° is

51

Figure 17 RMS elevation angle variations about surface correction model

a better measure of the uncertainty in the rms value estimate than the statistical confidence limits calculated from the number of degrees of freedom in the sample population.

The composite rms residual elevation variations about the surface model correction is also plotted in Figure 18 together with the increase in variance contributed by removing the surface correction (radar observations - no correction). The ratio between the corrected and uncorrected rms values is a measure of the effectiveness of the surface correction procedure. At 1° and above 7° true elevation angle, the observed variation of elevation angle error (no correction) is identical with the value expected from the simulation analysis. The observed rms fluctuations at elevation angles between 1° and 7° true elevation angle are as much as 40 percent higher than expected mirroring the influence of short term small scale refractive steering and internal atmospheric multipath discussed in Section 3.4.

Although all the variations of elevation angle error associated with surface refractivity variations were removed by the surface correction model, the model did not significantly reduce the variance. The rms fluctuations about the correction were only a factor of about 1.5 smaller than the uncorrected rms refraction fluctuations rather than the factor of 6 expected on the basis of the simulation analysis. The short term fluctuations which were not modeled and cannot be sensed by surface based techniques significantly affected the performance of the refraction correction model.

Summary results for the summer (June - August) and fall (September - November) time periods from the Haystack X-band observations (Crane, 1976b) are also plotted on Figure 18. These residual fluctuations are relative to a best fit third degree polynomial; any bias effect has been removed. They provide a measure of the minimum possible rms fluctuation. The Haystack observations are for 5 minute and 1 hour observation periods. The IDCSP satellites used as beacon sources for the Haystack observations were in 14 day orbits; the apparent elevation angle changed by approximately 1 degree per hour. The 1 hour fluctuations should correspond to the fluctuations to be expected within the 1 degree analysis interval used for the L-band radar observations. From Figure 18, it is evident that the rms variations about the surface correction model are of the
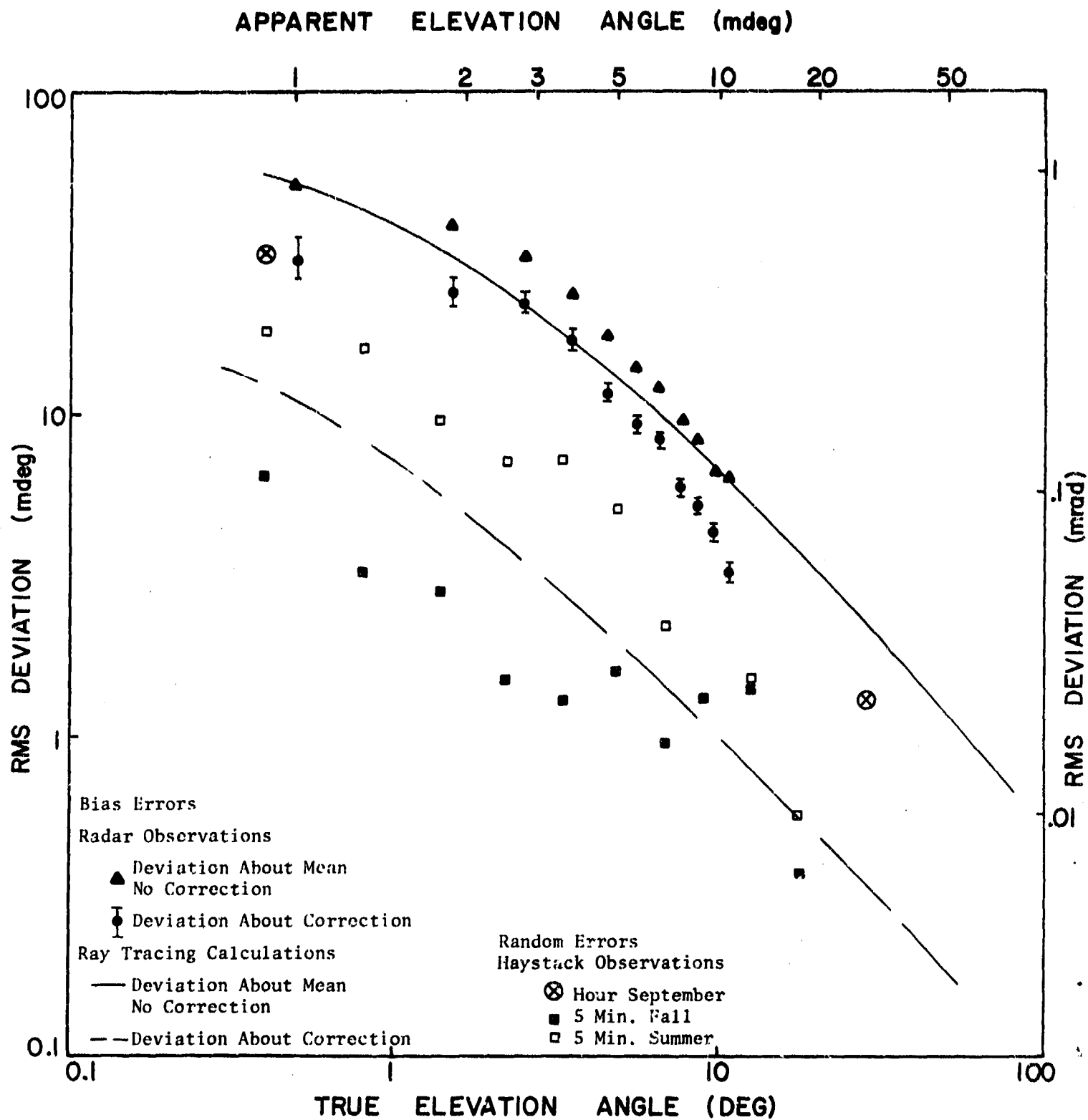
53

Figure 18   RMS elevation angle variations

same order of magnitude as the one hour fluctuations of the September 1975 Haystack data. These fluctuations are caused by small scale turbulence or by bouyancy waves on the inversion layer capping the planetary boundary layer.

The small scale nature of the perturbations is evident in the cross section variations (see Section 3.4 and Figures 3-5) which accompany the angle-of-arrival fluctuations. Large scale horizontal inhomogeneities such as modeled by Gallop and Telford (1975) could produce angle-of-arrival errors not correlated with surface refractivity but could not produce the accompanying cross section variations. The uncorrected variance represented by the deviations of the radar observations about correction are composed of contributions by both large and small scale irregularities. The effect of the large scale irregularities may be reduced by the addition of radiometric observations as proposed by Gallop and Telford; the small scale fluctuations cannot be reduced by such a technique. It is noted that the large scale irregularities will affect observations of point and distributed sources (such as the sun) in the same manner. The small scale irregularities will affect only observations of point targets such as the radar observations of satellites or observations of beacon sources. This difference between observations of point and distributed sources is responsible for the difference between the results reported here and the results reported by Anway (1963). Anway reported that the correlation coefficient between elevation angle error observations and surface refractivity at an elevation angle of $8°$ was 0.87 for observations of the sun. The radar observations result in a correlation coefficient of only 0.61 (see Table 3), the smaller correlation value being caused by the small scale irregularities.

6. CONCLUSIONS

The results of the low elevation angle tropospheric refraction effects program are that the ray-tracing model simulations of refraction effects are in agreement with observations of the average observed values. The variance of the observations about the simulated correction value based on measured surface refractivity was significantly larger than expected. The observed variations about the correction model were also larger than previously reported by Anway (1963). The departure of the measurements reported by Anway from the surface correction model can be attributed to the effects of large scale horizontal variations in refractive index, the problem described by Gallop and Telford (1975). The increase in variance about the correction model observed in this study was comparable to the variance about the mean value of elevation error observed within an hour and previously reported by Crane (1976b). The source of this increased variability relative to the results reported by Anway is small scale refractive index gradients which affect observations of point source targets but which do not affect the observations of distributed sources such as the sun.

The effects of small scale refractive gradient induced elevation angle errors cannot be reduced by regression model correction schemes using surface refractivity, surface based radiometry or a combination of both techniques. At this time these fluctuations, the rms residuals after correction displayed in Figure 18, represent the uncorrectable limitation to low elevation angle radar observations of targets at heights in excess of 1000 km (removal of the effects of large scale horizontal inhomogenities will not significantly reduce the variances displayed in Figure 18; the effect of large scale irregularities have already been eliminated from the Haystack data by the processing procedures used to prepare those data). It is further noted that these residual errors cannot be removed by correction using ray tracings of simultaneously acquired radiosonde profile data since the radiosonde data do not contain sufficient information to evaluate the effects of small scale refractivity gradients at the time of a radar measurement.

ACKNOWLEDGMENTS

REFERENCES

Anway, A.C. (1963): "Empirical Determination of Total Atmospheric Refraction at Centimeter Wavelengths by Radiometric Means", J. of Res. NBS, 670, (Radio Propagation), 153-160.

Bauer, J.R., W.C. Mason and F.A. Wilson (1958): "Radio Refraction in a Cool Exponential Atmosphere", Tech. Rept. 186, Lincoln Laboratory, MIT.

Bean, B.R. and G.D. Thayer (1954): "CRPL Exponential Reference Atmosphere", NBS Monograph 4, Central Radio Propagation Lab., Nat. Bureau of Standards, Boulder, Colorado.

Bean, B.R. and G.D. Thayer (1963): "Comparison of Observed Atmospheric Radio Refraction Effects with Values Predicted Through the Use of Surface Weather Observations", J. of Res. NBS, 67D, (Radio Propagation), 273-285.

Bean, B.R., B.A. Cahoon, and G.D. Thayer (1960): "Tables for the Statistical Prediction of Radio Ray Bending and Elevation Angle Errors Using Surface Values of the Refractive Index", NBS Tech. Note 44, Central Radio Propagation Lab., Nat. Bureau of Standards, Boulder, Colorado.

Born, M. and E. Wolf (1964): Principles of Optics, Pergamon Press, New York, Section 3.

Crane, R.K. (1971): "Description of the Avon-to-Westford Experiment", Tech. Rept. 483, Lincoln Laboratory, MIT.

Crane, R.K. (1976a): "Refraction Effects in the Neutral Atmosphere", in Methods of Experimental Physics, Vol. 12, Astrophysics, Part B, Radio Telescopes, M.L. Meeks (editor), Academic Press, New York, 186-200.

Crane, R.K. (1976b): "Low Elevation Angle Measurement Limitations Imposed by the Troposphere: An Analysis of Scintillation Observations Made at Haystack and Millstone", Tech. Rept. 518, Lincoln Laboratory, MIT.

DOD (1966): "Department of Defense World Geodetic System 1966", Tech. Report published by the Department of Air Force Aeronautical Chart and Information Center.

ESSA (1966): "U.S. Standard Atmosphere Supplements", ESSA, NASA, and the U.S. Air Force, U.S. Government Printing Office, Washington, D.C.

Evans, J.V. (1969): "The Millstone Hill Propagation Study", Tech. Note 1969-51, Lincoln Laboratory, MIT.

Evans, J.V. (1973a): "Millstone Hill Radar Propagation Study: Scientific Results, Parts I, II and III", Tech. Rept. 509, Lincoln Laboratory, MIT.

Evans, J.V. (1973b): "Millstone Hill Radar Propagation Study: Calibration", Tech. Rept. 508, Lincoln Laboratory, MIT.

Freehafer, J.E. (1951): "Geometrical Optics" in Propagation of Short Radio Waves, D.E. Kerr (editor), McGraw-Hill Book Co., New York, 41-58.

Gallop, M.A., Jr. and L.E. Telford (1975): "Use of Atmospheric Emission to Estimate Refractive Errors in a Non-Horizontally Stratified Troposphere", Radio Sci., 10, 935-945.

Ghiloni, J.C. (1973): "Millstone Hill Radar Propagation Study: Instrumentation", Tech. Rept. 507, Lincoln Laboratory, MIT.

TRW (1966): "Functional Specifications of Lincoln Laboratory Orbit Determination Programs", TRW Systems, prepared under Lincoln Laboratory, MIT Contract BB202.

MISSION
of
Rome Air Development Center

RADC plans and executes research, development, test and selected acquisition programs in support of Command, Control Communications and Intelligence (C^3I) activities. Technical and engineering support within areas of technical competence is provided to ESD Program Offices (POs) and other ESD elements. The principal technical mission areas are communications, electromagnetic guidance and control, surveillance of ground and aerospace objects, intelligence data collection and handling, information system technology, ionospheric propagation, solid state sciences, microwave physics and electronic reliability, maintainability and compatibility.